City Research Online

City, University of London Institutional Repository

Permanent repository link: https://openaccess.city.ac.uk/id/eprint/22445/

Link to published version: http://dx.doi.org/10.1002/eqe.3169

DIRECT ESTIMATION OF SEISMIC RESPONSE IN REDUCED-DEGREE-OF-FREEDOM ISOLATION AND ENERGY DISSIPATION SYSTEMS

Konstantinos I. Gkatzogias[1], and Andreas J. Kappos[1, 2]

[1]Research Centre for Civil Engineering Structures, Civil Engineering Department, City, University of London, UK

[2]Civil Engineering Department, Aristotle University of Thessaloniki, Greece

A methodology for the development of design tools for direct estimation of peak inelastic response in reduced-degree-of-freedom (RDOF) isolation and energy dissipation systems is presented. The suggested procedure is an extension of an earlier method addressing purely hysteretic isolation systems. Herein, the dynamic equation of motion is first normalised to reduce the number of design parameters that significantly affect the response. The sensitivity of normalised response quantities to the amplitude of the ground motion is then investigated through extensive parametric nonlinear dynamic analyses of isolated single-degree-of-freedom (SDOF) systems with linear viscous damping using code-based target spectra. Regression analysis is subsequently employed to develop generalised design equations (GDEs) suitable for design. Further investigations are made to address nonlinear viscous damping and the effect of the transverse component of seismic action in two-degree-of freedom (2DOF) systems under bidirectional excitation, making the procedure applicable to common bridge isolation schemes. GDEs constitute an alternative to equivalent linearisation approaches commonly adopted by codes, informing the selection among alternative isolation and energy dissipations schemes without requiring iterative analysis. The approach is incorporated in the *Deformation-Based Design* methodology for seismically isolated bridges in a forthcoming paper.

KEYWORDS

Seismic isolation, bridges, nonlinear dynamic analysis, viscous dampers, unidirectional/bidirectional excitation, Eurocode 8

1. INTRODUCTION

Implementation of structural control principles to mitigate undesirable vibrations of dynamically excited civil engineering structures in seismically-prone areas has attracted the attention of the research community in the last four decades resulting in diverse types of control devices.[1] Passive base isolation (elastomer-based, sliding-based), supplementary energy dissipation (hysteretic, viscoelastic) devices, and typically combinations thereof, represent currently the norm in seismic structural control applications to bridges. The diversity of the available hardware, in terms of mechanical properties and induced modification of structural response, introduces additional challenges in the formulation of performance-based methodologies. Challenges refer to (*i*) accommodating the use of a broad class of devices, and (*ii*) providing design guidelines to inform the initial selection and comparative evaluation of alternative isolation and energy dissipation schemes under different performance levels, considering various design constraints and the associated cost.

Practice-oriented bridge design methods adopting standard equivalent linearisation approaches (i.e. based[2] on the effective period and equivalent damping ratio at peak response) provide some partial guidance in this respect by setting a target inelastic displacement and/or equivalent damping ratio at the start of the procedure. Yet, criteria for selecting these values cannot be easily identified and, in any case, the effective period and equivalent damping ratio are not proper indicators for damage in the substructure of seismically isolated bridges. In fact, the design of the isolated structure under the base shear associated with the target displacement and equivalent viscous damping ratio (i.e. the definition of strength) constitutes the last step of the so-called 'direct displacement-based design' approach.[2] Ideally, preliminary selection criteria should address the displacement and energy dissipation capacity of the isolation system as a function of the shear transmitted through the isolation interface, thus indicating the cost of the substructure design. Some useful, albeit crude, guidance in this direction (along with some criteria for selecting the type of devices) is occasionally provided,[3] using high-damping elastic spectra in the pseudo-acceleration vs. displacement response spectra format, disregarding the contribution of viscous dampers to peak inertia forces transmitted to the substructure. More refined direct approaches, based on nonlinear static[4] and response history analysis[5–7] (NLRHA), may be capable of facilitating preliminary selection of the hardware considering design requirements from different performance

levels. However, these approaches are currently restricted to specific types of devices/structures (e.g. structures isolated through bilinear hysteretic isolators,[5,6] non-isolated yielding frames with dampers[4,7]), hence they do not readily meet the needs of design of isolated bridges. On the other hand, codes[8–10] do not provide specific recommendations regarding the above issues. Quite the contrary, the integration of equivalent linearisation approaches is typically employed in a format that introduces iterations as a means to evaluate the response of a preselected passive system (e.g. based on engineering judgement). This 'indirect' format along with the consideration of the variability of design properties of devices, leave the designer with the heavy task of conducting numerous analyses when the performance of different isolation schemes and/or multiple design constraints and performance levels are investigated.

Despite the aforementioned high computational effort, the accuracy of results may not be ensured. Research studies explicitly addressing isolated bridges (or systems that may approximate the response of bridges) led in the past to contradictory findings[11,12] regarding the appropriateness of the equivalent linearisation. A more recent work[13] questioned the rationality of using the 'non-physical' effective period to describe the period of vibration, proposing instead the isolation period that corresponds to the post-yield stiffness of the isolation system as a more efficient indicator of maximum response. Various studies (e.g. [2,14–16]) proposed different definitions of the equivalent damping ratio to improve accuracy, while other researchers[17,18] concluded that standard definitions based on geometric considerations result in reasonable estimates of peak inelastic response. Conflicting results regarding the ability of equivalent linearisation to predict the inelastic response under bidirectional excitation (e.g. adoption of the common '100%+30%' combination rule[8]) were also reported.[5,19,20] Relevant deviations resulting from the implementation[19,20] of the equivalent linearisation as prescribed by US codes were recently attributed[21] to the selection–scaling of records, the definition of the target spectrum under bidirectional excitation and the adopted measure of central tendency. An additional inherent limitation of linearisation procedures lies in their inability to capture the peak total inertia forces at the critical state of peak total acceleration (i.e. forces transferred to the substructure), and the peak damping forces at the state of peak relative velocity (i.e. viscous damper forces), unless the main dissipative source of the isolation system has a purely hysteretic behaviour. The issue emerges from the deviation of peak total acceleration and relative velocity from their respective pseudo-counterparts[22] and it has been addressed by various research groups (e.g. [17,23]). Although research focused on the efficiency of equivalent linearisation approaches in isolated bridges with viscous dampers is relatively scarce, several studies addressed this with reference to yielding building structures, and to a certain degree, conclusions regarding SDOF systems (e.g. [17]) were found to be applicable to isolated bridges.[24] Irrespective of the accuracy/inaccuracy of equivalent linearisation approaches, the evaluation of which is beyond the scope of this study, the above issues shed a certain scepticism on the efficiency of equivalent linearisation or at least on the proper format to be adopted.

In view of the previous considerations, a methodology for the direct estimation of peak inelastic response in RDOF isolation and energy dissipation systems is put forward here. An accurate, yet practical and transparent, design route is sought. The starting point is a procedure previously developed by Ryan and Chopra[5,6] for bilinear hysteretic isolation systems, disregarding viscous damping. The method involved (*i*) normalisation of the dynamic equation of motion with a view to uncoupling the response from the amplitude of ground motion and minimising the dispersion in peak normalised relative displacements, and (*ii*) development of design equations by statistically processing NLRHA results derived from the previous step. The proposed methodology extends the normalisation to address a broader range of seismic isolation systems that may consist of linear and bilinear isolators (e.g. low or high-damping elastomeric bearings (LDRB/HDRBs), lead-rubber bearings (LRBs), supplementary energy dissipation devices (i.e. linear (LVDs) and nonlinear viscous dampers (NLVDs)), as well as combinations thereof, hence encompassing most isolation schemes commonly used in modern bridges. GDEs are developed for the direct estimation of both peak relative displacements and total accelerations, addressing only parameters of 'engineering significance', representative of seismic isolators and dampers (i.e. instead of 'effective' properties). Derived equations further aim at the identification of 'near-optimal' characteristics of the isolation and energy dissipation system in terms of performance and cost under both unidirectional and bidirectional excitation. In this context, the term 'direct' is used herein to emphasise practicality. Specifically, GDEs may be used to predict the response of a system with given properties or plot response curves for various system properties. Relevant charts facilitate the selection of the basic characteristics of the isolation system and the substructure (unknown at the start of the design process) and the comparative evaluation of alternative isolation and energy dissipation schemes. Different performance levels, variable design properties of devices, and/or other design constraints, may be considered with no need to perform iterative analysis. 'Design principles' involving use of design (target) spectra and code-compatible scaling procedures are also introduced, allowing the interpretation of results derived from different types of analysis implemented according to Eurocode 8 (EC8).[8,25]

The procedure consists of the steps summarised in Figure 1 and explained in detail in Sections 2 to 5 for alternative RDOF systems. The analysis framework is first presented in Section 2 including the definition of target spectra associated with different PLs, alternative representation of seismic actions, and modelling issues. Following the suggested normalisation procedure, the dynamic equation of motion is parametrically solved. Regression analysis is finally employed to develop GDEs. SDOF systems with linear damping are first considered in Section 3. The procedure is subsequently extended to address nonlinear viscous damping (Section 4), as well as the effect of the transverse component of seismic action (Section 5). The methodology can be used to extract GDEs for code-prescribed target spectra which in turn can be provided as ready-to-use tools for the direct estimation of inelastic response. Alternatively, the procedure may be easily automated with a view to developing regression models when spectra of 'user-defined' frequency content are adopted.
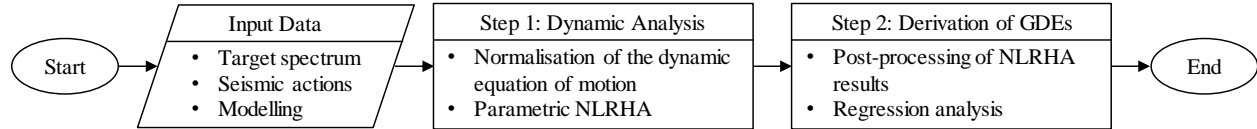
```
┌────────┐    ╱ Input Data      ╱   ┌─ Step 1: Dynamic Analysis ─┐   ┌─ Step 2: Derivation of GDEs ─┐   ┌──────┐
│ Start  │──▶╱ • Target spectrum ╱──▶│ • Normalisation of the dynamic │▶│ • Post-processing of NLRHA │──▶│ End  │
└────────┘  ╱ • Seismic actions ╱    │   equation of motion       │   │   results                    │   └──────┘
           ╱ • Modelling       ╱     │ • Parametric NLRHA         │   │ • Regression analysis        │
                                     └────────────────────────────┘   └──────────────────────────────┘
```

Figure 1 Development of GDEs for the direct estimation of peak response

2. ANALYSIS FRAMEWORK

2.1. Target Spectra and Representation of Seismic Action

Any type of design spectrum (code-type or resulting from site-specific hazard analysis or zonation study) can be used as the target spectrum. Herein, the EN1998–1[25] 'Type 1' 5%-damped elastic spectrum for site conditions 'C' is selected to demonstrate the suggested approach, as shown in Figure 2A for unidirectional excitation (denoted as 1D). However, a significant modification compared to the Eurocode elastic response spectrum was made. In line with recent research findings,[26] the corner period defining the beginning of the constant displacement response range of the spectrum was set equal to $T_D = 4.0$ s as a more representative value of high seismicity regions compared to the recommended[25] $T_D = 2.0$ s. The adopted period is also in line with the minimum value in ASCE/SEI 7–16 standard[10] that specifies values up to 16 s. Identifying the importance of displacements in the design of isolated bridges, EN1998–2[8] allows similarly the specification of a T_D value that is longer than the value prescribed in the National Annex to EN1998–1.[25]

Assuming that the level of seismic action (EQ) is defined in terms of the reference peak ground acceleration (PGA)[25] $\ddot{u}_{g,max,ref}$, the modification factor γ_{EQ} (the importance factor according to EC8 terminology) required to scale the reference seismic action with a return period $T_{R,ref}$ to a different period T_R was approximated as $(T_{R,ref} / T_R)^{-1/k}$. The value of the k exponent expresses the slope of a linear (in logarithmic space) approximation of the hazard curve at the site ranging between 1.5 and 4.5. Its exact value depends on both the seismicity of the region and the spectral ordinate considered.[26] Herein a constant value of 2.4 was adopted while the corresponding γ_{EQ} was uniformly applied to the reference target spectrum whenever a seismic action of different probability level was sought, assuming a constant shape of the target spectrum regardless of the intensity of the earthquake. The 'constant shape' assumption, although strictly not valid, enables the use of the same design equations irrespective of the performance level under consideration, since, as it will be shown in Sections 3–5, the formulation of GDEs depends on the frequency content rather than the amplitude of the ground motion. The target spectrum under bidirectional excitation (denoted as 2D) was represented by the square root of the sum of squares (SRSS) of the target spectra per horizontal direction assuming unidirectional excitation, resulting in $\sqrt{2}EQ_{ref}$ for the reference seismic action in line with EN1998–2[8] ('Target' in Figure 2C). Although this may be considered a rather conservative approach, it was selected herein with a view to assessing the expected increase in peak inelastic response when records are scaled according to the code (Section 5).

NLRHAs presented in the following sections were performed under different ensembles of artificial and natural records. The primary objective in both cases of records was the reliable estimation of the mean response under a seismic excitation that matches as closely as feasible the 'design excitation' (i.e. the target spectrum) rather than the accurate estimation of the variability in seismic response around this mean. Artificial accelerogram generation was based on the well-established Gasparini and Vanmarcke[27] approach using the Saragoni and Hart[28] envelope function with a total duration of 25 s and time step of 0.01 s. The approach for artificial motion generation was selected due to its simplicity and widespread adoption in practice, and is consistent with the provisions of modern codes like Eurocode

8 (CEN 2004) [25] for artificial records; nevertheless, different procedures may be employed. Three alternative suites were generated[29] to fit the reference target spectrum, namely, Art A[30], B (Figure 2A), and C[30], consisting of 5, 10, and 20 artificial records, respectively; the records were properly scaled using γ_{EQ} to represent seismic actions associated with different return periods. To investigate the effect of the transverse component of seismic action in bidirectional excitation using artificial records, an additional suite (Art D)[30] was formed by arranging the previously generated acceleration histories in 10 pairs of horizontal components (H1, H2). In line with the concept of principal axes,[31] each pair was characterised by a near-zero correlation coefficient[30] and an intensity ratio of the horizontal component spectra equal to 0.75 for far-field ground motions and long vibration periods (i.e. > 1.5 s)[32]. Consistency to the 2D target spectrum was established by scaling H1 and H2 with the scaling factors $\gamma_{H1}=1.13\gamma_{EQ}$ and $\gamma_{H2}=085\gamma_{EQ}$ that maintain the adopted intensity ratio. Geometric means (GMs) of ground motion intensity parameters, i.e. PGA, peak ground velocity (PGV), displacement (PGD), and Arias intensity (I_A) for suites of records are also presented in Figure 2A for Art B.
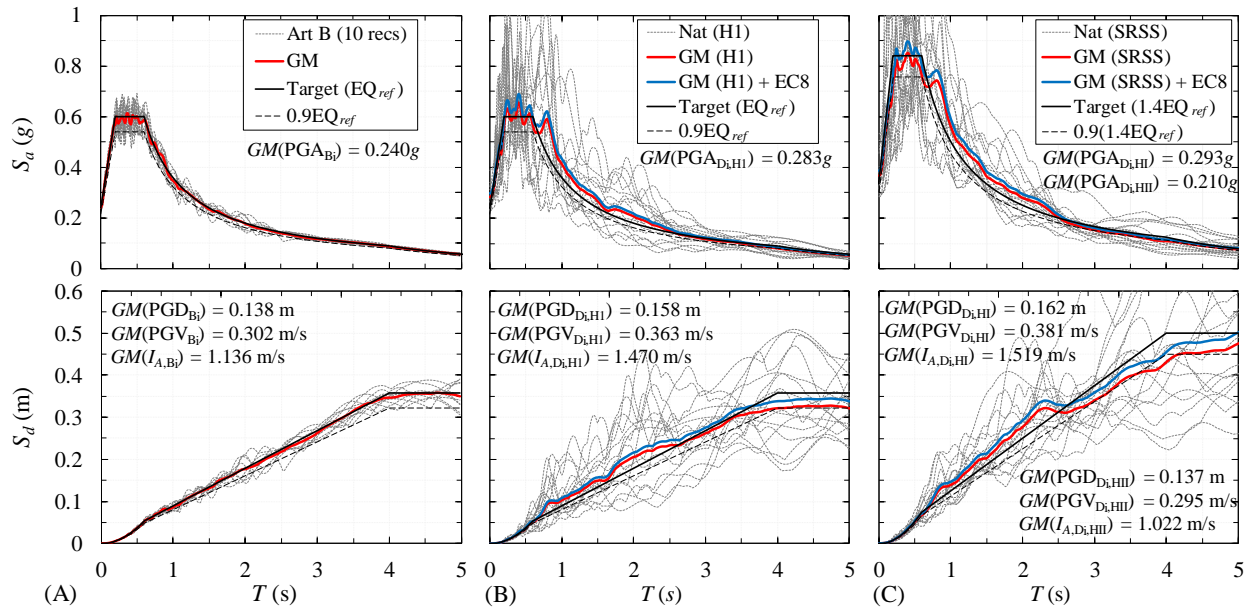

Figure 2 Spectral matching of response acceleration S_a and displacement S_d geometric mean (GM) and EN1998–2-scaled[8] geometric mean (GM+EC) spectra to the: (A) 1D target spectrum (site 'C', $T_{R,ref}=475$ yrs) for Art B artificial records ($\gamma_{EQ}=1.0$), (B) 1D target spectrum for γ_{MSE}-scaled natural (Nat) records considering H1 components ($\gamma_{EC8}=1.05$), and (C) 2D target spectrum for rotated and γ_{MSE}-scaled Nat records ($\gamma_{EC8}=1.05$)

Selection and scaling of natural records aimed at forming a suite for assessment purposes with a mean spectrum that closely matches the target spectrum while suppressing the variability in structural response (hence increasing reliability), since the uncertainty of the input motion is already incorporated in the definition of the target spectrum.[33] Eligible pairs of seismic events were initially selected from the PEER NGA–West 2 (http://ngawest2.berkeley.edu/) database.[34] Adopted preliminary search criteria were moment magnitude $M_w = 6.5$~7.0, closest distance from the record site to the ruptured area $R_{rup} = 20$~40km, average shear wave velocity to a depth of 30 m $V_{s,30} = 180$~360 m/s (corresponding to site conditions 'C'[25]), and lowest usable frequency 0.2 Hz. The sample of eligible events was further constrained by assessing the similarity of spectra of the selected records to the target spectrum over the entire period range. The overall fit was quantified by the mean-square-error (MSE) of the differences between the spectral accelerations of the record (or the SRSS spectrum of the pair of records) and the 1D (or 2D) target spectrum. A local (i.e. per record or pair of records) scaling factor γ_{MSE} was calculated so that MSE was minimised over the considered period range.[35] Adopting an allowable γ_{MSE} of 0.7~2.5 and employing the above procedure initially for the H1 components[34] and subsequently for the pairs of horizontal components of the NGA preliminarily selected pairs, resulted in the suite of 16 eligible records[30] presented in Figure 2B, C for analysis under uni/bidirectional excitation. In the case of bidirectional excitation, the horizontal components of selected events were rotated into their principal axes defined as the axes along which the two horizontal components are uncorrelated and assumed statistically independent.[31] The major principal axis (I) is defined as the one parallel to the major principal component (HI), i.e.

the component with the larger I_A, as opposed to the minor principal axis (II) and component (HII) (smaller I_A). The counter-clockwise rotation angle (for which the correlation coefficient between two unrotated acceleration histories is zero) and the rotated acceleration histories, were calculated according to Rezaeian and Der Kiureghian.[36]

Ground motion intensity and energy characteristics of the γ_{MSE}-scaled records presented in Figure 2B, C incorporate (similarly to Figure 2A) the site ('C') amplification factor S_C, i.e. intensity parameters are comparable to $S_C = 1.15$ times the peak ground characteristics of the target spectra. Overall, they present a good match to the relevant values derived in the case of artificial records, noting however, their superiority in terms of both intensity and energy (PGV, I_A). Finally, according to the EC8 requirement, the ensemble spectra depicted in Figure 2 were scaled by a global (i.e. per suite) scaling factor γ_{EC8} (equal to unity in the case of artificial records) to ensure that their spectral values are not lower than 0.9 times the target spectra[8] over the entire period range (i.e. $0 \leq T_i \leq 5$ s). In view of the previous considerations, the scaling factor γ per record and per probability of exceedance is determined as $\gamma_{EQ}\gamma_{MSE}\gamma_{EC8}$. The design (or target) value of PGV $\dot{u}_{g,max}$, required during the development of GDEs, was selected herein equal to the geometric mean of PGVs of the records included in Art B suite (i.e. 0.302 m/s for $T_R = 475$ yrs). The above decision was driven first from the fact that the selected value was close to the mean PGV derived from relationships proposed in recent research studies (varying from 0.244 to 0.345 with a mean of 0.301 m/s)[30] compared to the rather unconservative estimate provided by EN1998–2[8] (i.e. 0.225 m/s). Second, it was driven from a prerequisite of the methodology presented in Sections 3–5, to use records with an ensemble spectrum that closely matches the target spectrum in terms of shape and PGV; the issue is further discussed in Section 3.2.

2.2. Numerical Evaluation and Statistical Processing of Key Response Quantities

Response history analyses (RHAs) in Sections 3–5 were performed using the unconditionally stable implicit Newmark constant average acceleration method.[37] The procedure was fully automated with the developed *MATLAB*[38] code *IDEC* (*Isolation Design Equations Code*) that enables parametric nonlinear dynamic analysis of RDOFs using *RUAUMOKO 3D*[37] and *DYNAPLOT*[39] in batch mode. *IDEC* further performs post-processing of results involving data collection, statistical processing, regression analysis, development of GDEs, and diagram plotting, with average time of less than 5 s per analysis and post-processing of a single case, using an 8 GB RAM 2.20 GHz quad core processor.

A bilinear hysteretic element and a dashpot element were used to model the inelastic force–displacement response of isolators and viscous dampers according to Figure 3. The considered SDOF system idealises an isolated straight bridge with a rigid deck of total mass m under unidirectional excitation. The deck is mounted on a single isolator of hysteretic force–displacement response and a single viscous damper, representing the combined response of bridge isolators and dampers, respectively, while the effects of the substructure's stiffness, inertial, and damping characteristics, are disregarded. The restoring shear force (V) of the bilinear isolator can be described[40,41] by Equation 1, where $u(t)$ represents the displacement history, k_p the post-elastic stiffness (associated with the isolation period T_p), and V_0 the shear resistance of the isolator at zero displacement (hereafter termed 'isolation system strength' for brevity). $z(t)$ is a hysteretic dimensionless parameter[40,41] governed by the evolution Equation 2 (i.e. a function of u, relative velocity $\dot{u}$, and the initial stiffness k_e). Defining the fraction of the applied V_0 (maxima of ± 1) or else the 'yielding history',[5] $|z(t)| = 1$ when the system enters the inelastic range and < 1 otherwise (i.e. elastic response). In Equation 2 u_y represents the yield displacement and s controls the smoothness of the transition from the elastic to the inelastic range in the V–u relationship; for $s = 8$ a sharp transition is obtained. For V_0 equal to zero the hysteretic response collapses to linear behaviour with stiffness equal to k_p;

$$V(t) = V_0 z(t) + k_p u(t) \tag{1}$$

$$\dot{z} = \left(\dot{u}(t) - 0.5|\dot{u}(t)| z(t) |z(t)|^{s-1} - 0.5\dot{u}(t)|z(t)|^{s}\right)/u_y \tag{2}$$

The behaviour of the bilinear isolator is intrinsically determined by three parameters, which can be selected as V_0, u_y, and k_p. u_y was reported in earlier studies (e.g. [42,43]) to have a minor impact on the maximum inelastic response; herein a constant value associated with different groups of yielding isolators was introduced[5,6] in order to capture more accurately the peak response, and at the same time limit the complexity of the proposed GDEs. In addition, u_y was considered constant[5] for different values of the post-yield stiffness k_p (i.e. instead of assuming a constant ratio of k_e / k_p) resulting to an initial stiffness ($k_e = V_0$ / $u_y + k_p$) that is directly proportional to the yield strength ($V_y = k_e u_y$) (i.e. k_e and V_y expressed as functions of V_0, u_y, k_p to define the bilinear hysteresis for modelling purposes).
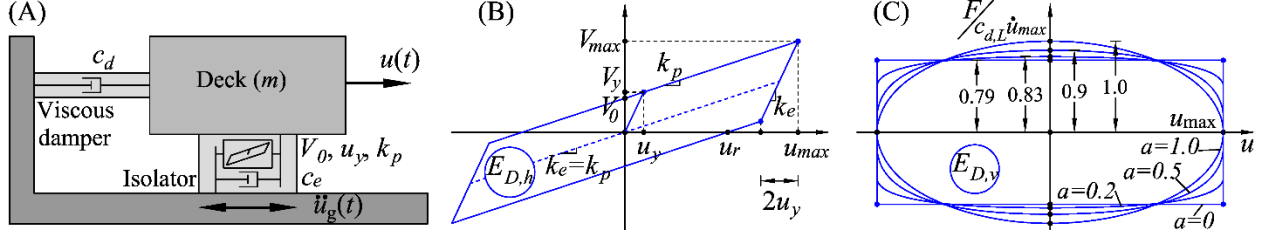
Figure 3 (A) Idealised SDOF system; force–displacement response of (B) bilinear hysteretic isolator, and (C) linear (a=1) and nonlinear (a<1) viscous dampers of equal dissipated energy under a cycle of harmonic motion

The axial force (F) in the general case of NLVDs can be expressed[44] as a fractional velocity power law as per Equation 3, where $c_{d,NL}$ is the damping coefficient, a is a real positive velocity coefficient with typical values for seismic applications in the range of 0.1~1, and sgn($\cdot$) is the sign function.

$$F_{NL}(t) = c_{d,NL} \, \text{sgn}\left(\dot{u}(t)\right)\left|\dot{u}(t)\right|^{a} \tag{3}$$

The energy dissipated by the nonlinear damper during a cycle of harmonic motion $u = u_{max}\sin\omega t$ of exciting frequency ω and peak relative displacement u_{max}, is calculated[44] as $E_{D,v,NL} = \pi c_{d,NL} u_{max}^{a+1}\omega^a f(\Gamma, a)$ where $f(\Gamma, a)$ represents a function of the velocity exponent a and the gamma function $\Gamma(\cdot)$. Introducing $a = 0$ and $a = 1$, Equations 3 and $E_{D,v,NL}$ collapse to the limit cases of pure friction ($F_{NL}(t) = c_{d,NL}\text{sgn}\dot{u}(t)$, $E_{D,v,NL} = 4c_{d,NL}u_{max}$) and linear viscous dampers ($F_L(t) = c_{d,L}\dot{u}(t)$, $E_{D,v,L} = \pi c_{d,L}u_{max}^2\omega$). The effect of the nonlinear parameter a on the response envelope is illustrated in Figure 3C where $F / c_d\dot{u}_{max}$ (i.e. F normalised to the peak damper force) is plotted against $u = u_{max}\sin\omega t$.

The response of NLVDs was investigated in this study following the 'energy-equivalence' approach[44,45] according to which energy-equivalent dampers are characterised by two dimensionless and independent parameters. These are the parameter a and the equivalent damping ratio $\xi_{d,NL}$, associated with the degree of nonlinearity and the energy dissipation capacity, respectively. Equating $E_{D,v,NL}$ to $E_{D,v,L}$ yields $c_{d,NL}$ for an energy-equivalent nonlinear damper[45] (i.e. dissipating energy equal to the energy of the linear damper);

$$c_{d,NL} = \frac{\left(u_{max}\omega\right)^{1-a}}{f(\Gamma,\alpha)}c_{d,L} = \frac{\left(u_{max}\omega\right)^{1-a}\,\pi\Gamma\left(2+\alpha\right)}{2^{2+a}\Gamma^2\left(1+\alpha/2\right)}c_{d,L} \tag{4}$$

Substituting $c_{d,NL}$ in Equation 3 yields $F_{0,NL}$ for the energy-equivalent nonlinear damper and the associated ratio of peak damper forces[45] $F_{0,NL} / F_{0,L} = (u_{max}\omega / \dot{u}_{max})^{1-a} / f(\Gamma, a)$. For energy-equivalent dampers of $a = 0, 0.2, 0.5, 1$, under harmonic motion ($\dot{u}_{max} = \omega u_{max}$), $F_{0,NL} / F_{0,L}$ results in the peak force reductions depicted in Figure 3C. In the case of an SDOF system under non-harmonic excitation, the response should be assessed[22] at $\omega = \omega_p$ (i.e. the system's isolated frequency associated with k_p), and the ratio of forces depends additionally on the ratio of the pseudo-velocity $u_{max}\omega_p$ to the peak relative velocity $\dot{u}_{max}$.

Considering again the SDOF system of mass m, isolation frequency ω_p, and a nonlinear viscous damper of $c_{d,NL}$, the equivalent damping ratio $\xi_{d,NL}$ can be expressed[44,45] by Equation 5 using the definition of $E_{D,v,NL}$ and $\omega = \omega_p$. For $a = 0$ and $a = 1$ the equivalent damping ratio reduces to $\xi_{d,NL} = 2c_{d,NL} / \pi k_p u_{max}$ and $\xi_{d,L} = c_{d,L} / 2m\omega_p$, respectively.

$$\xi_{d,NL} = \frac{E_{D,v,NL}}{2\pi k_p u_{max}^2} = \frac{c_{d,NL}}{2m\omega_p}\frac{f(\Gamma,\alpha)}{\left(u_{max}\omega_p\right)^{1-a}} \tag{5}$$

In summary, different isolation schemes can be realised by properly combining the modelling parameters describing the force–displacement response of the bilinear hysteretic and dashpot element, i.e. V_0, k_p, u_y, ξ, and a. In the following sections, the dynamic response retrieved from analysis of isolation and energy dissipation systems under a suite of records is characterised by the *geometric mean* (*GM*) of responses under individual records (or pairs of records in bidirectional analysis), and the *standard error of the geometric mean* (*SEGM*) estimate.[30] *GM* is preferred

over the more common arithmetic mean mainly due to its consistency with lognormally distributed data, i.e. an assumption which was found to be realistic for earthquake response quantities. Nevertheless, the above decision has a minor effect on results so long as a consistent definition of the central tendency is adopted both on scaling of accelerograms and analysis results processing.[46] The standard error of the sample geometric mean estimate is the standard deviation of the sampling distribution of the geometric mean and represents the dispersion of sample-means around the true (i.e. the population) geometric mean. $SEGM$ is used here to assess the reliability of the GM prediction.

In the case that the sample size is small (i.e. number of records $n < 30$), exact confidence intervals of the geometric mean estimate are first calculated.[30] Considering an $(1 - a_s)$% confidence level (CL) and $n - 1$ degrees of freedom df for the two-sided *Student-t* probability density function, the lower (L) and upper (U) geometric mean intervals are given as $GM_{U/L} = \exp[\ln GM \pm \delta \cdot t(a_s/2, df) / (n - 1)^{0.5}]$. δ is the sample standard deviation of the natural logarithms of response quantities, the *t*-factor depends on the CL assigned to predict the response estimate, and a_s represents the significance level. Associated $SEGM$ limits defined as percentages of the estimated GM can be subsequently retrieved as $SEGM_{U/L}$ (%) $= \pm |GM_{U/L} - GM| \cdot 100 / GM$. In the analyses presented in Sections 3–5, peak absolute seismic response quantities (i.e. peak relative displacement and total acceleration) are of interest, hence, reported $SEGM$ (%) values correspond to the upper (and more conservative) confidence interval. As an example of interpretation of the provided $SEGM$ values, a sample of n peak relative displacements resulted from dynamic analysis of an isolated system under a suite of n records ($df = n - 1$), a confidence level of 90%, a sample geometric mean GM, and $SEGM_{U/L}$ limits, are assumed. If one were to construct many response samples of n displacements drawn from the same population, and the standard deviation of the samples remained constant, approximately 90% of the $\pm SEGM_{U/L}$ confidence intervals (which would differ for each sample) would encompass the true mean. Alternatively expressed,[33] the sample-mean peak relative displacement is estimated with a confidence band of approximately $\pm SEGM_{U/L}$. A limit value of $SEGM = 15$% of GM with a 90% confidence level[33] was adopted herein to assess the accuracy of the mean estimates rather than introduce an increase in values derived from analysis.

3. ISOLATED SDOF WITH LINEAR VISCOUS DAMPING

3.1. Dynamic Equation of Motion

The dynamic equation of motion of the SDOF system is recast here to a form that permits uncoupling the response from the amplitude of the ground motion and thus linearising the problem. The key advancement in this procedure is the explicit consideration of linear viscous damping, while in earlier studies[5,6] viscous damping was ignored. Applying *D'Alembert*'s principle using the shear force of the bilinear isolator $V_0(t)$ and the axial force of the LVD $F_L(t)$ (Section 2.2), the differential equation governing the response of the idealised SDOF is written as:

$$\ddot{u}(t) + \left[\left(\left(c_{e,L} + c_{d,L} \right)/m \right) \dot{u}(t) \right] + \left[\bar{v}_0 g z\left(t, k_e, u, \dot{u}\right) + \omega_p^2 u(t) \right] = -\ddot{u}_g(t) \tag{6}$$

In Equation 6, $\ddot{u}(t)$ is the relative acceleration of *m*. $c_{e,L}$, $c_{d,L}$ that are associated with viscous damping originating from the rubber of elastomer-based isolators (i.e. linear) and LVDs, respectively, represent 'quantifiable' sources of damping, hence, they are kept constant[47] during NLRHA as opposed to the 'unquantifiable' inherent structural damping of the deck and substructure. Inherent damping is deliberately disregarded on the basis that neither the deck nor the pier deformations are associated with the *u* dynamic degree of freedom (Figure 3A). *u* represents the horizontal relative displacement of the rigid (i.e. undeformed) deck or else the deformation of the isolation system, excluding the effect (i.e. deformations) of the substructure. $\bar{v}_0$ represents the strength (at zero displacement) of the hysteretic part of the isolator normalised to the weight of the superstructure $V_0 / (mg)$, i.e. the seismic coefficient (where g is the acceleration of gravity); it can be also seen[5] as the acceleration at yield of a rigid-plastic system with strength V_0. The maximum residual displacement u_r under which the system can be in static equilibrium (Figure 3B), corresponding to a shear force of $\pm 2V_0$ and representing a system property (i.e. independent of the excitation), is equal to V_0 / k_p. Dividing Equation 6 by u_r and substituting $c_{e,L}$, $c_{d,L}$ ($= 2m\omega_p \xi_L$) and $\bar{v}_0$, reduce the equation of motion to the normalised form of Equations 7, 8 (symbols with bars represent normalised quantities);

$$\bar{\ddot{u}}(t) + \left[2\omega_p \left(\xi_{e,L} + \xi_{d,L} \right) \bar{\dot{u}}(t) \right] + \left[\omega_p^2 \left(z\left(t, k_e, u, \dot{u}\right) + \bar{u}(t) \right) \right] = -\left(\omega_p^2 / \eta \omega_D \right) \bar{\ddot{u}}_g(t) \tag{7}$$

$$\bar{\ddot{u}}(t) = \ddot{u}(t)/u_r , \quad \bar{\dot{u}}(t) = \dot{u}(t)/u_r , \quad \bar{u}(t) = u(t)/u_r , \quad \bar{\ddot{u}}_g(t) = \ddot{u}_g(t)/\dot{u}_{g,max} \tag{8}$$

The normalised strength η, which describes the isolation system strength relative to the PGV, is defined[5] according to Equation 9, where the frequency ω_D included to render η a dimensionless quantity corresponds to T_D;

$$\eta = \bar{v}_0 g \big/ \left(\omega_D \dot{u}_{g,\max} \right) = \omega_p^2 u_r \big/ \left(\omega_D \dot{u}_{g,\max} \right) \tag{9}$$

The characterisation of the isolation system strength by η along with the consideration of a constant u_y, reduce the governing parameters that influence the response to T_p, η, and ξ_L ($= \xi_{e,L} + \xi_{d,L}$), as opposed to the parameters T_p, V_0, c_L ($= c_{e,L} + c_{d,L}$), u_y, $\dot{u}_{g,\max}$ in the non-normalised case. Specifically, Equation 7 indicates that the normalised response is independent of the ground motion amplitude, rendering u, $\dot{u}$, $\ddot{u}$ linearly proportional to u_r according to Equation 8. The numerical study in Sections 3.2, 3.3 investigates the validity of the previous statement in typical isolation schemes with linear viscous damping, and explores its practical value in design with the aid of statistical analysis.

3.2. Parametric Analysis of SDOF System

Normalised relative displacements $\bar{u}(t)$ and total accelerations $\bar{\ddot{U}}(t)$ can be found either directly by solving Equation 7 for selected values of ξ, η, ω_p (or T_p), and u_y, or indirectly by first solving Equation 6 with the corresponding values c_L, V_0, k_p, and then by calculating the normalised response from Equation 8. In the latter case, k_p is given as $4\pi^2 m / T_p^2$ and V_0 is calculated from rearranging Equation 9. In both cases, $\dot{u}_{g,\max}$ represents the scaled PGV of the considered record; for a specific value of η this results in a variation of $\bar{v}_0$ with ground motion intensity (i.e. per record) according to Equation 9. Geometric means of peak normalised relative displacements $\bar{u}_{\max}$, total accelerations $\bar{\ddot{U}}_{\max}$, logarithmically transformed response quantities $\ln\bar{u}_{\max}$, $\ln\bar{\ddot{U}}_{\max}$ (i.e. natural logarithms), and non-normalised peak relative displacements $u_{\max}$ and total accelerations $\ddot{U}_{\max}$ under Art B motions are presented in Figure 4. Response values are provided for a range of design parameters, i.e. $\xi_{e,L} = 0.05$, $\xi_{d,L} = 0\sim0.25$, $\eta = 0\sim1.5$, $T_p = 1\sim5$ s. Considering $T_D = 4$ s, the mean PGV for Art B (i.e. $\dot{u}_{g,\max} = 0.604$ m/s for $T_R \approx 2500$ yrs), and $\bar{v}_0 = 0\sim0.15$, Equation 9 yields an approximate range of η from 0 to 1.50; larger η values are expected if lower seismic intensities are considered, noting however, that in the latter case low $\bar{v}_0$ values will be normally selected. The yield displacement u_y is considered equal to 10 mm representing the case of elastomer-based hysteretic isolators (e.g. LRBs)[5] while the viscous damping ratio ξ_e and ξ_d were dealt as a single variable due to the inherent linearity of the system. An issue that requires some further consideration in the case of linear systems is the computation of normalised response quantities; zero strength (i.e. $\eta = \bar{v}_0 = 0$) results in zero u_r rendering impossible the derivation of $\bar{u}(t)$, $\bar{\ddot{U}}(t)$ according to Equation 8. The issue was
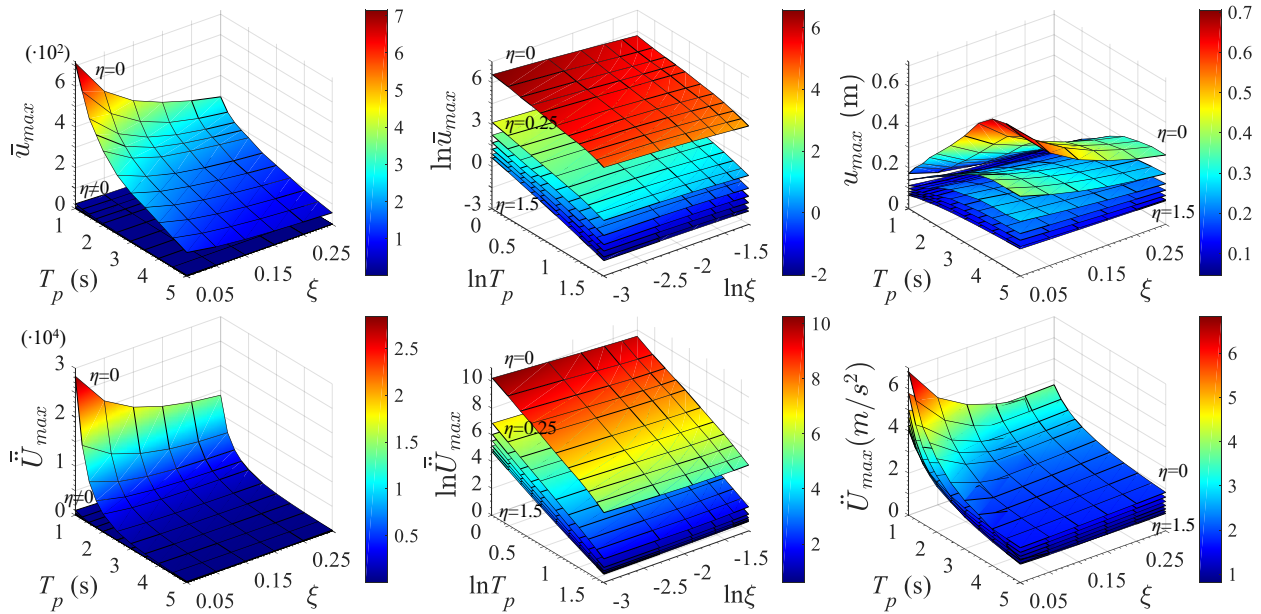

Figure 4 NLRHA results under Art B suite: *GM*s of $\bar{u}_{\max}$, $\bar{\ddot{U}}_{\max}$, $\ln\bar{u}_{\max}$, $\ln\bar{\ddot{U}}_{\max}$, $u_{\max}$, $\ddot{U}_{\max}$ for PGA of 0.42g ($T_R \approx 2500$ yrs, $\gamma_{EQ}=2$) at bedrock

treated numerically by adopting $\eta = 0$ when solving Equation 6 and a relatively low value of $\eta = 0.01$ when calculating the normalised response, since the system response was found almost insensitive to such a small increase in strength.

Each surface in Figure 4 represents a three-dimensional spectrum associated with a specific value of η. Top surfaces ($\eta = 0$) of normalised data are located at a greater distance compared to the cases of $\eta \neq 0.01$ due to the normalisation with respect to a relatively small value of u_r. Dispersion[30] δ, and hence $SEGM$, for non-normalised response depends on the generation and/or scaling approach adopted for the considered suite of records, while in the case of normalised response the normalisation procedure of Section 3.1 is equivalent, in terms of δ, to scaling of records to a common PGV. In other words, if records were scaled to the same PGV, δ and $SEGM$ for u_{max}, $\bar{u}_{max}$ and $\ddot{U}_{max}$, $\ddot{\bar{U}}_{max}$ would be identical. In Figure 5, $SEGM$ for normalised and non-normalised response estimates are plotted for different values of ξ, η, T_p. Upper values of $SEGM$ are close to 15% with a 90% CL in the case of $\bar{u}_{max}$ and lower than 10% in the case of $\ddot{\bar{U}}_{max}$, corresponding to values of δ lower than 0.25 and 0.20, respectively, which in turn are lower than those reported[5] for bilinear isolation systems disregarding viscous damping (0.3~0.6 referring to $\bar{u}_{max}$). Although such low values of $SEGM$ imply a reliable mean response estimation, it should be noted that statistical processing of non-normalised response results in similar $SEGM$ values (Figure 5) due to the low scattering of artificial spectra around their mean (and target) values (Figure 2A).
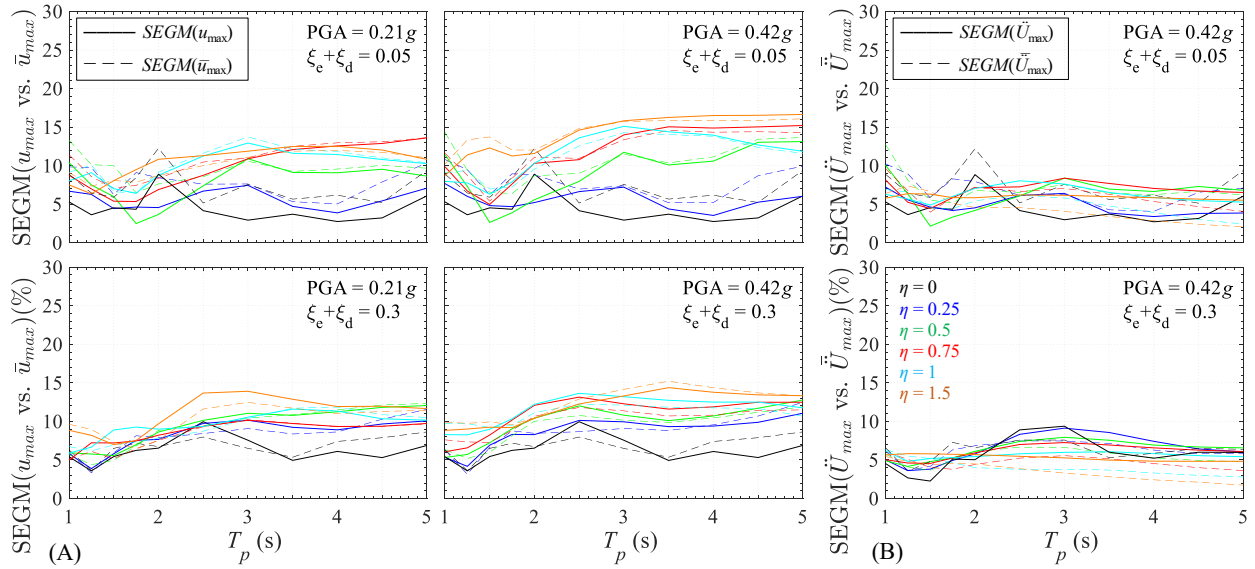

Figure 5 NLRHA results under Art B suite: $SEGM$ (%) for (A) u_{max}, $\bar{u}_{max}$, and (B) $\ddot{U}_{max}$, $\ddot{\bar{U}}_{max}$, for PGAs of $0.21g$ (T_R=475 yrs, γ_{EQ}=1), $0.42g$ ($T_R \approx$2500 yrs, γ_{EQ}=2) at bedrock, ξ=5, 30%, and η=0~1.5

In view of the previous considerations, the main advantage of the normalisation approach lies in the fact that the ground motion amplitude has indeed a negligible effect on the mean normalised peak response of linear/nonlinear isolation systems with/without supplemental linear viscous damping. The effect is illustrated in Figure 6 for two different seismic intensities. A minor influence of the increased intensity is evident only in the displacement response of systems with increased η and/or short T_p that are of little interest in seismic isolation of bridges. Values of $SEGM$ for $\bar{u}_{max}$ that are insensitive to the increase of seismic intensity (Figure 5A) support the above statement. The combination of increased reliability in mean response estimation and the independence of the normalised response from the amplitude of ground motion allows the development of GDEs.

Prior to proceeding to the aforementioned task, the effect of the number and type of accelerograms on the normalised/non-normalised response was investigated. To this purpose, the procedure described earlier was repeated using Art A, C, and Nat(H1) (γ_{EC8} = 1) suites of artificial and natural records. Normalised response quantities $\bar{u}_{max}$, $\ddot{\bar{U}}_{max}$ are first plotted in Figure 7A revealing some divergence from the Art B suite response, mainly in the case of displacements under Nat(H1). Deviation of curves in plots of normalised response are attributed primarily to the 'goodness-of-fit' of the GM spectrum of the selected records to the target spectrum, since the normalised inelastic spectra of Figure 7A are disengaged from the effect of the amplitude of ground motion. Shifting from the normalised
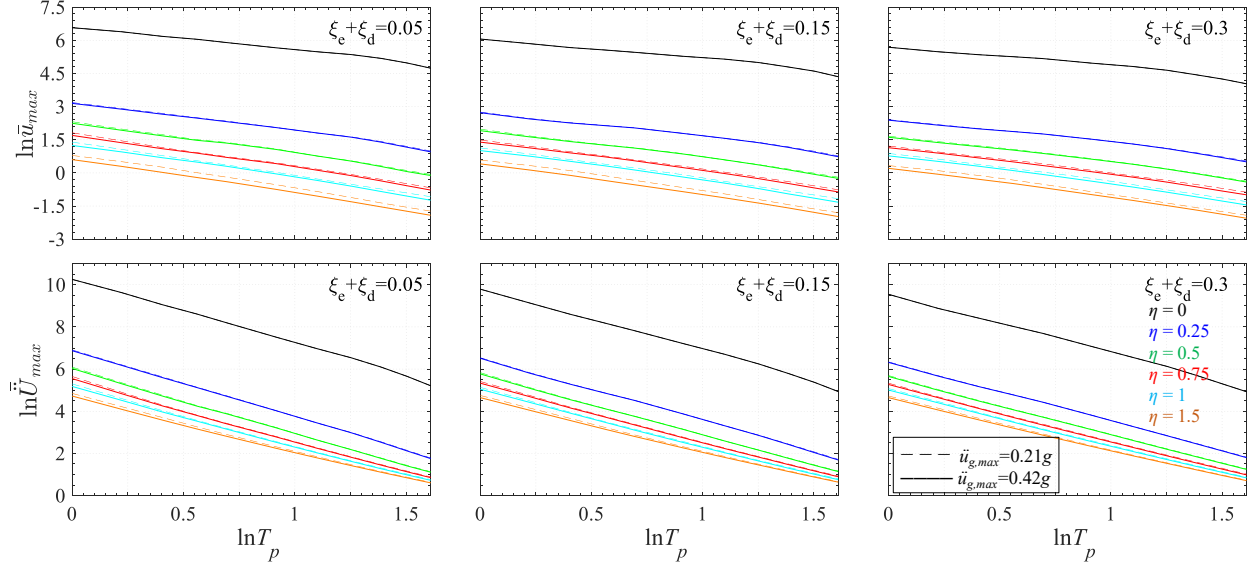
Figure 6 NLRHA results under Art B suite: *GM* of $\ln\bar{u}_{max}$ and $\ln\bar{\bar{U}}_{max}$ for PGAs of 0.21g (T_R=475 yrs, γ_{EQ}=1), 0.42g ($T_R\approx$2500 yrs, γ_{EQ}=2) at bedrock, ξ=5, 15, 30%, and η=0~1.5
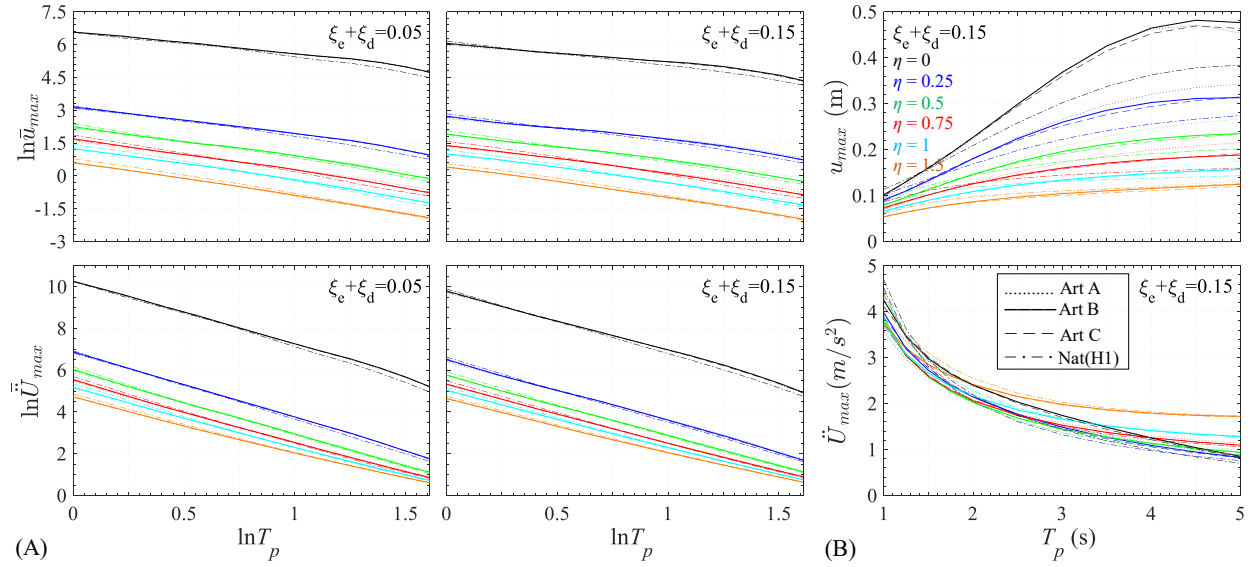

Figure 7 NLRHA results under Art A, Art B, Art C, Nat(H1) (γ_{EC8}=1): *GM* of (A) $\ln\bar{u}_{max}$, $\ln\bar{\bar{U}}_{max}$, and (B) u_{max}, $\ddot{U}_{max}$ for PGA of 0.42g ($T_R\approx$2500 yrs, γ_{EQ}=2) at bedrock, ξ=5, 15%, and η=0~1.5

response to non-normalised one, requires the definition of a target (or design) value for PGV. Adopting, as discussed earlier in Section 2.1, a design value of PGV equal to the *GM* of PGVs of records included in Art B (i.e. 0.302 m/s for T_R = 475 yrs), results in the non-normalised response presented in Figure 7B for $T_R \approx 2500$ yrs and ξ = 15%. In this case (i.e. non-normalised response), the accuracy in mean response estimation will depend, in addition to 'goodness-of-fit' to the target spectrum, on the degree of matching of the design PGV to the *GM* of the PGVs of the individual records. This is valid for the suites of artificial records and especially Art B resulting in response estimates that clearly follow the target spectra in the case of ξ = 5%, η = 0, and T_R = 475 yrs (Figure 8A). It is also seen (Figure 7) that the number of records in the case of artificial records does not have a significant effect on the estimated response; only the Art A (5 records) curves seem to slightly diverge from Art B results. On the other hand, the suite of natural records underestimates relative displacements and total accelerations for low values of ξ and η, due to the adoption of a design PGV that is lower than the *GM* of record PGVs (i.e. 0.363m/s for T_R = 475 yrs). The underestimation of response

further distorts the spectral matching depicted in Figure 2B and implies that a larger number of natural records (i.e. >16) may be required to describe more efficiently the shape and the design PGV of the target spectra. These trends derive from a marked difference between the Ryan and Chopra[5,6] approach and the extended method presented herein. The former uses a number of records associated with a specific seismic scenario to determine a target spectrum and a design PGV, while the latter sets a (code/site-specific) target spectrum (and design PGV) as the starting point, and requires the selection of spectrum and intensity compatible records.

To assess the reliability of mean response estimates, *SEGM* for normalised response was calculated for the considered suites. In general, *SEGM* for $\bar{u}_{max}$ was found more difficult to be limited within a preselected value, herein ±15% of *GM* with a 90% *CL*, compared to *SEGM* for $\ddot{\bar{U}}_{max}$. The resulted standard deviation of inelastic response under Art A (i.e. $\delta \approx 0.3$ and 0.25 for $\bar{u}_{max}$ and $\ddot{\bar{U}}_{max}$, respectively) imply that even when artificial records are used, more than 5 records may be required to constraint *SEGM* for $\bar{u}_{max}$. Nevertheless, satisfactory results will still be obtained, according to Figure 7, leading to some conservatism in u_{max}, as opposed to the unconservative estimates derived from the Nat(H1) suite. In the case of natural records, the resulting peak *SEGM* values for $\bar{u}_{max}$, $\ddot{\bar{U}}_{max}$ are constrained approximately below 20% corresponding to δ values of 0.4. Such values remain at the lower limit of those reported in Ryan and Chopra,[5] indicating the effectiveness of the normalisation procedure of Section 3.1 but also the need for a larger number of records to attain the predefined degree of reliability. Considering the degree of complexity and the computational effort involved when natural records are used to derive the normalised response (i.e. selecting records compatible with the shape and PGV of code-based target spectra, scarcity of recorded accelerograms, increased number of analyses), GDEs are hereafter developed for Art B. Artificial records can easily satisfy the above requirements and provide robust estimates of mean response within a deterministic design framework disregarding member strength degradation (which is reasonable in seismically designed bridges).[8] The inherent variability of natural records can be considered at a later stage of design using a more refined type of analysis as in the *Deformation-Based Design* method that will be presented in a forthcoming paper.

3.3. Derivation of Generalised Design Equations

Uncoupling the response from the amplitude of ground motion allows the development of GDEs that can provide direct estimates of $\bar{u}_{max}$ and $\ddot{\bar{U}}_{max}$ as a function of ξ, η, T_p, irrespective of the performance level and associated seismic action under consideration. The problem can be tackled by developing regression models extending to a 3D-space (T_p–ξ–η). To this end, linear regression equations were fitted to the logarithmically transformed normalised response derived from NLRHAs as it was found that $\ln\bar{u}_{max}$ and $\ln\ddot{\bar{U}}_{max}$ vary almost linearly with $\ln\xi$ and $\ln T_p$ (Figure 4). Different linear regression models using three independent predictors (i.e. ξ, η, T_p) were developed for $\bar{u}_{max}$ and $\ddot{\bar{U}}_{max}$ since peak total accelerations (and hence maximum forces $m\ddot{U}_{max}$) in the isolation and energy dissipation system cannot be directly associated with peak relative displacements (due to the introduction of ξ in general higher than 5%). Although complex regression models can be derived using the *IDEC* code, an effort was made to simplify the relevant design equations with a view to increasing their usefulness in practical design, therefore different GDEs were extracted for linear ($\eta = 0$) and nonlinear systems ($\eta \neq 0$).

High-degree polynomials are first fitted to the normalised response variable $\bar{y}$ (i.e. $\bar{u}_{max}$ or $\ddot{\bar{U}}_{max}$) resulting in GDEs of the general form of Equation 10 for a complete *m*-degree polynomial with *q* terms, where *j*, *k*, *l* indices are permuted accordingly, and b_i coefficients are estimated using the method of least squares. Stepwise regression is finally employed to assess the statistical significance of terms using the *R*-squared criterion[38] and reduce the total number of terms in the model. u_{max} and $\ddot{U}_{max}$ response can be subsequently predicted by transforming Equation 10 to the non-normalised space by analogy to Equation 8. GDEs in the form of $y = u_r\exp(\ln \bar{y})$ provide direct estimates of u_{max} and $\ddot{U}_{max}$ under different PLs associated with target spectra of common frequency content but different amplitude.

$$\ln \bar{y}_m \left(\ln \xi, \ln \eta, \ln T_P \right) = \sum_{i=0}^{m} b_i \left(\ln \xi \right)^j \left(\ln \eta \right)^k \left(\ln T_P \right)^l , \quad \begin{array}{l} j+k+l \leq i \\ q=(m+1)(m+2)(m+3)/6 \end{array} \tag{10}$$

The 'goodness-of-fit' of the regression models was assessed both in terms of limiting the divergence of the predicted response from analysis results (i.e. residuals), and identifying 'near-optimal' isolation systems under different seismic intensities. A 'near-optimal' isolation system[48] is defined herein as the one that results in 'near-minimum' peak total acceleration $\ddot{U}_{max}$. Representative results of different *m*-degree regression models (RM) with *q* terms ($m \times q$) are presented in Figure 8 for two different seismic intensities associated with $T_R = 2500$ yrs and $T_R = $

475 yrs. The intensity associated with 2500 yrs was used to develop the regression models, and the second to assess the robustness of models in predicting estimates of non-normalised response under a different intensity of ground motion. As expected, models of $\eta = 0$ were found[30] to predict response quantities under different earthquake intensities with the same accuracy due to their inherent linearity. In general, all models present excellent fit and the larger divergence is mainly associated either with the upper limit of the considered period range (i.e. $T_p = 5$ s) (which is not common even in isolated bridges) or with low values of u_{max} and $\ddot{U}_{max}$. Nevertheless, when the terms in the regression equations are significantly reduced, the resulting models fail to predict the shape (or curvature) of displacement and acceleration curves. This is of particular importance when identification of 'near-optimal' isolation systems is additionally sought by the adopted model, and is more conveniently illustrated by plotting the inelastic spectra in a $u_{max}-\bar{v}_0$, $\ddot{U}_{max}-\bar{v}_0$ format (Figure 9) that facilitates the identification of isolation schemes (ξ, $\bar{v}_0$, T_p) with a 'near-optimal' performance (i.e. min $\ddot{U}_{max}$). $\ddot{U}_{max}$(opt) curves represent a visualisation of the design criterion of min $\ddot{U}_{max}$ per T_p, and u_{max}(opt) indicates the corresponding relative displacements of the isolation system, both plotted for the case of $\xi = 5\%$ where deviations from NLRHA are more significant and involve response quantities of higher magnitude. It is seen that RM2 can accurately capture the location of 'near-optimal' isolation systems for the range of $T_p = 1$~5s, however, the simpler RM3 model can also be adopted since it is deemed adequate for practical applications in bridge engineering (i.e. $T_p = 1.5$~4s). GDEs in the case of RM3 take the general form of Equations 11, 12 (simplified as shown in Table 1), wherein y represents either u_{max} or $\ddot{U}_{max}$, and the ground motion intensity is expressed for convenience in terms of PGA at bedrock, i.e. $\ddot{u}_{g,max}$ in m/s².
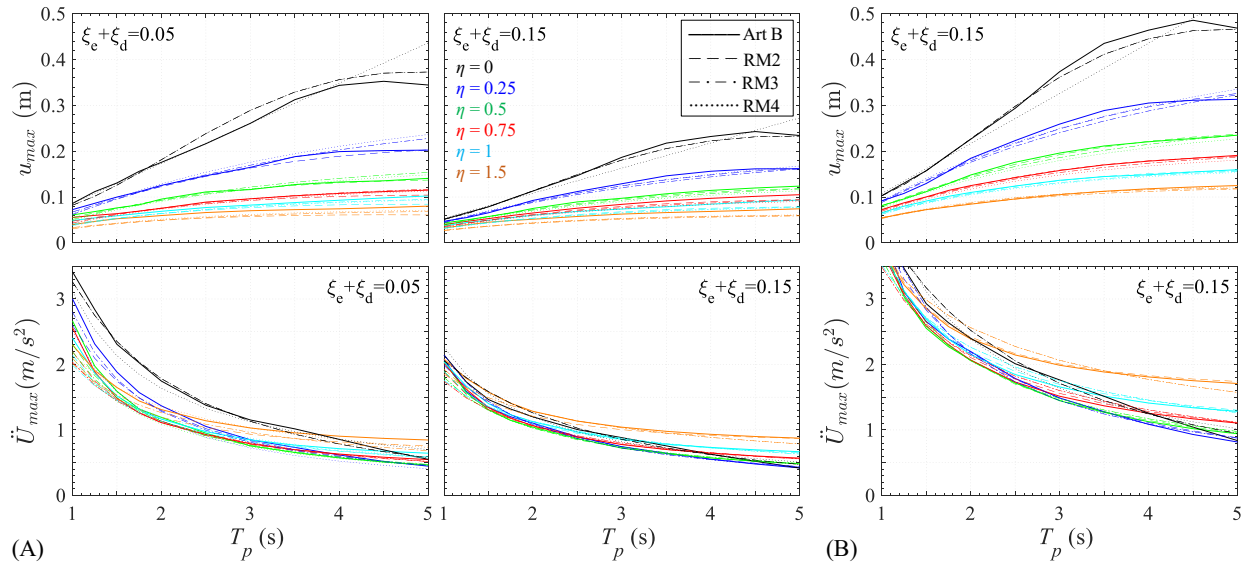
Figure 8 NLRHA response u_{max} and $\ddot{U}_{max}$ under Art B compared to response predicted from RM2, RM3, and RM4 for PGA of (A) 0.21g (T_R=475 yrs), and (B) 0.42g (T_R≈2500 yrs) at bedrock, ξ=5, 15%, η=0~1.5
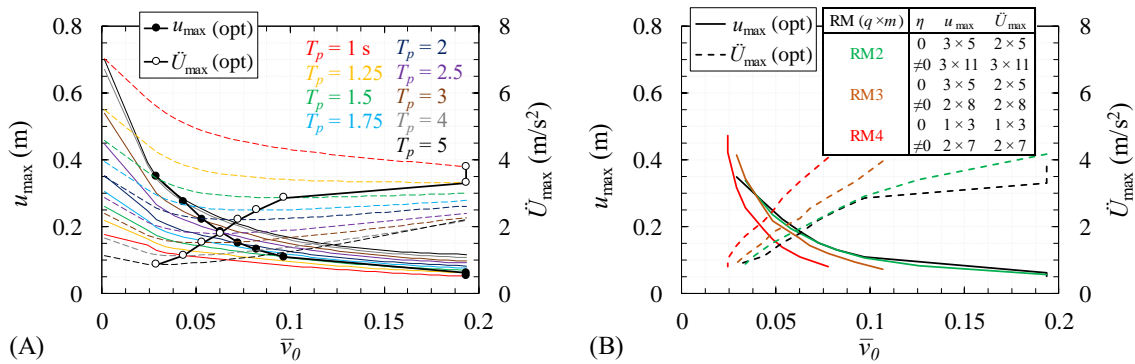
Figure 9 Optimal peak total accelerations $\ddot{U}_{max}$ (opt) and corresponding relative displacements u_{max} (opt) derived from (A) NLRHA under Art B, and (B) RM2, 3, 4, for PGA of 0.42g (T_R≈2500 yrs, γ_{EQ}=2) at bedrock, ξ=5%, 1D excitation

$$y = \frac{0.362e^{\text{Int}}}{2\pi g} \xi^{(\beta + \gamma \ln \eta + \delta \ln T_p)} \eta^{(1 + \varepsilon + \zeta \ln \eta + \kappa \ln T)} T_p^{(2 + \lambda + \mu \ln T_p + \nu (\ln T_p)^2)} \ddot{u}_{g,\max} \tag{11}$$

$$\eta = 4.31 \bar{v}_0 g / \ddot{u}_{g,\max} \tag{12}$$

Table 1 RM3 regression coefficients: EN1998–1, site conditions 'C'[25], 1D excitation

Case	y	Int	β	γ	δ	ε	ζ	κ	λ	μ	ν
$\eta = 0$	$u_{\max}$	5.245	-0.428	-	-	-	-	-	-1.194	0.797	-0.443
	$\ddot{U}_{\max}$	8.952	-0.419	-	0.150	-	-	-	-2.266	-0.226	-
$\eta = 0.25\text{-}1.5$	$u_{\max}$	0.623	-0.178	0.097	-	-1.192	-0.095	-0.175	-1.100	-0.209	-
	$\ddot{U}_{\max}$	4.769	-0.114	0.094	0.128	-0.754	0.153	0.255	-2.393	-	-

Since earlier studies[42,43] have demonstrated that the response of isolated structures is not sensitive to the exact value of u_y, the regression coefficients of Table 1 may also be used to approximately predict $u_{\max}$, $\ddot{U}_{\max}$ of isolation systems consisting of friction-based devices ($u_y < 1$mm). However, derivation of case-specific GDEs using *IDEC* is expected to yield finer response estimates primarily in terms of 'near-optimal' system identification. Likewise, GDEs presented here (and in Section 5) strictly refer to a frequency content associated with site conditions 'C'[25] and a period range of 1~5 s, somewhat broadened compared to the range of practical interest in the design of isolated bridges (1.5~4.0 s). Nevertheless, the procedure was fully automated within *IDEC* that can derive GDEs for 'user-defined' target spectra and period range, provided that a relatively small number of spectrum-compatible artificial records or (depending on the objective of the analysis) an ideally large number of natural records is specified (Section 3.2).

4. ISOLATED SDOF WITH NONLINEAR VISCOUS DAMPING

4.1. Dynamic Equation of Motion

The procedure described in Section 3.1 is extended here to study the effect of NLVDs on the peak response of isolated SDOFs. In this context, the dynamic equation of motion of the idealised system of Figure 3 is re-written using from Section 2.2 the expressions for the shear force of the bilinear isolator and the axial force of the LVD and NLVD;

$$\ddot{u}(t) + \left[\left(c_{e,L} \dot{u}(t) + c_{d,NL} \operatorname{sgn}(\dot{u}(t)) |\dot{u}(t)|^a \right) \big/ m \right] + \left[\bar{v}_0 gz(t, k_e, u, \dot{u}) + \omega_p^2 u(t) \right] = -\ddot{u}_g(t) \tag{13}$$

The constant viscous damping coefficient $c_{d,NL}$ (associated with NLVDs), is expressed by Equation 5 introducing the 'energy-equivalence' approach. The unknown term $u_{\max}$ required for the calculation of $c_{d,NL}$ when $a \neq 1$ (Equation 4), is defined here as the peak displacement of the SDOF with an energy-equivalent LVD of $\xi = \xi_{e,L} + \xi_{d,NL}$ and $a = 1$.

$$\ddot{u}(t) + \left[2\omega_p \xi_{e,L} \dot{u}(t) + \frac{2\omega_p \xi_{d,NL} \left(u_{\max} \omega_p \right)^{1-a}}{f(\Gamma, \alpha)} \operatorname{sgn}(\dot{u}(t)) |\dot{u}(t)|^a \right] + \left[\bar{v}_0 gz(t, k_e, u, \dot{u}) + \omega_p^2 u(t) \right] = -\ddot{u}_g(t) \tag{14}$$

The characterisation of NLVDs by the 'energy-equivalence' approach (i.e. dampers of the same ξ but different a) is introduced as the first of the two conditions required to uncouple the response from the ground motion amplitude. The second condition involves the characterisation of the isolation system strength by η as described in Section 3.1. Dividing Equation 14 by u_r, the equation of motion is reduced to the normalised form of Equations 8, 15;

$$\bar{\ddot{u}}(t) + \left[2\omega_p \xi_{e,L} \bar{\dot{u}}(t) + \frac{2\omega_p \xi_{d,NL} \left(\bar{u}_{\max} \omega_p \right)^{1-a}}{f(\Gamma, \alpha)} \operatorname{sgn}(\bar{\dot{u}}(t)) |\bar{\dot{u}}(t)|^a \right] + \left[\omega_p^2 \left(z(t, k_e, u, \dot{u}) + \bar{u}(t) \right) \right] = -\left(\omega_p^2 / \eta \omega_D \right) \bar{\ddot{u}}_g(t) \tag{15}$$

The normalised equation of motion along with the consideration of a constant u_y, reduce the governing parameters that influence the response to T_p, η, ξ ($= \xi_{e,L} + \xi_{d,NL}$), and the nonlinear parameter a, as opposed to T_p, V_0, $c_{e,L}$, $c_{d,NL}$, a, u_y, $\ddot{u}_{g0}$ in the non-normalised case, indicating that the normalised response is independent of the amplitude. The validity of this statement along with the effect of nonlinearity of viscous dampers are explored in the following section.

4.2. Parametric Analysis of SDOF System and Generalised Design Equations

A numerical study is performed herein by calculating the normalised response of representative isolation and energy dissipation systems for a range of design parameters (i.e. $\xi_{e,L} = 0.05$, $\xi_{d,NL} = 0\sim0.25$, $\eta = 0\sim1.5$, $T_p = 1\sim5$s, $a = 0.2\sim1$, $u_y = 10$ mm) under the Art B suite. In case the nonlinearity parameter a equals unity, Equation 15 is simplified to Equation 7 (i.e. linear viscous damping) and Section 3.2 applies. Statistical processing of parametric analysis results revealed that the range and trends of *SEGM* in $\bar{u}_{max}$, $\ddot{\bar{U}}_{max}$ curves in Figure 5 are not significantly affected by the value of the nonlinearity parameter of viscous dampers, implying small differences in u_{max} and $\ddot{U}_{max}$ compared to the case of linear viscous damping ($a = 1$). Furthermore, it was found[30] that the ground motion amplitude has a negligible effect on the mean normalised response irrespective of the degree of the nonlinearity of viscous dampers. In other words the reduction of the velocity exponent a in Equation 15 reduces the maximum axial damper force (Figure 3C) without significantly affecting the system's overall response (i.e. $\bar{u}_{max}$, $\ddot{\bar{U}}_{max}$). A minor influence of the intensity is mainly evident in the displacement response of systems with increased η and/or short T_p, similarly to Figure 6 (i.e. regardless of the a value). The negligible effect of a on the peak inelastic response is clearly illustrated in Figure 10A where the non-normalised u_{max}, $\ddot{U}_{max}$ response is evaluated for energy-equivalent damper systems of $a = 0.2$, 0.4, 0.6, 1.0, different values of η, and total damping ratio of $\xi = 0.15$, 0.30. It is seen that the influence of damper nonlinearity on the displacement response becomes stronger as $\xi_{d,NL}$ increases and a reduces. Specifically, considering the case of $\xi = 0.30$, divergences (Div) in the range of -15% and +12.5% are displayed between the $a = 1$, and $a = 0.2$ cases of displacement response (Figure 10B). Exact values depend on η and T_p but are relatively insensitive to the ground motion intensity (not shown in the figure), while Divu_{max} further reduces to ±10% with the increase of a to 0.4. Total accelerations are even less affected, exhibiting values of Div$\ddot{U}_{max}$ within -7.5~5% in the case of $a = 0.2$, and -7.5~2.5% in the case of $a = 0.4$. Useful from a design point of view is the remark that as ξ increases, positive Div values (indicating increase in seismic response due to the introduction of nonlinearity in viscous damping) are mainly observed for long T_p in the case of u_{max}, short T_p in the case of $\ddot{U}_{max}$, and increased values of η in both u_{max} and $\ddot{U}_{max}$ cases.
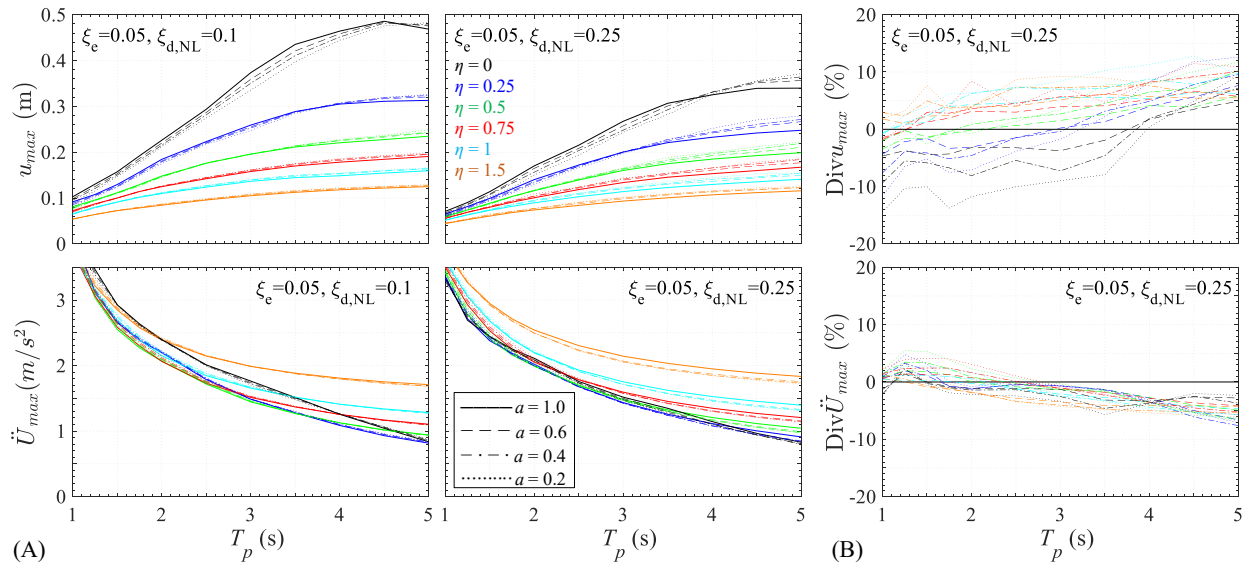

Figure 10 NLRHA results under Art B: (A) *GM* of u_{max}, $\ddot{U}_{max}$ considering energy-equivalent dampers of a=1, 0.6, 0.4, 0.2; (B) Div of u_{max}, $\ddot{U}_{max}$ from a=1 in the case of a=0.6, 0.4, 0.2 for PGA of 0.42g (T_R≈2500 yrs, γ_{EQ}=2) at bedrock

The independence of the normalised response from the ground motion amplitude combined with increased reliability in mean response estimation, allows the development of GDEs following the procedure described in Section 3.3. Nevertheless, as discussed above, the introduction of nonlinearity in viscous dampers was found to have a minor

effect on the overall response of different isolation and energy dissipation systems with maximum divergence response rates mainly associated with low displacement amplitudes at short periods (Figure 10). Hence, the parameters influencing the $\bar{u}_{\max}$, $\ddot{\bar{U}}_{\max}$ response can be further reduced to ξ ($= \xi_{e,L} + \xi_{d,NL}$), η, and T_p, (i.e. excluding a), resulting in the regression model and GDEs that were developed earlier in Section 3.3, and thus limiting the complexity of design equations. The effectiveness of the RM3 model in predicting the inelastic response in the case of systems with nonlinear viscous damping is demonstrated in Figure 11, where response quantities predicted by GDEs (Table 1) are compared with analysis results derived for $a = 1$ and $a = 0.2$ under two different seismic intensities.
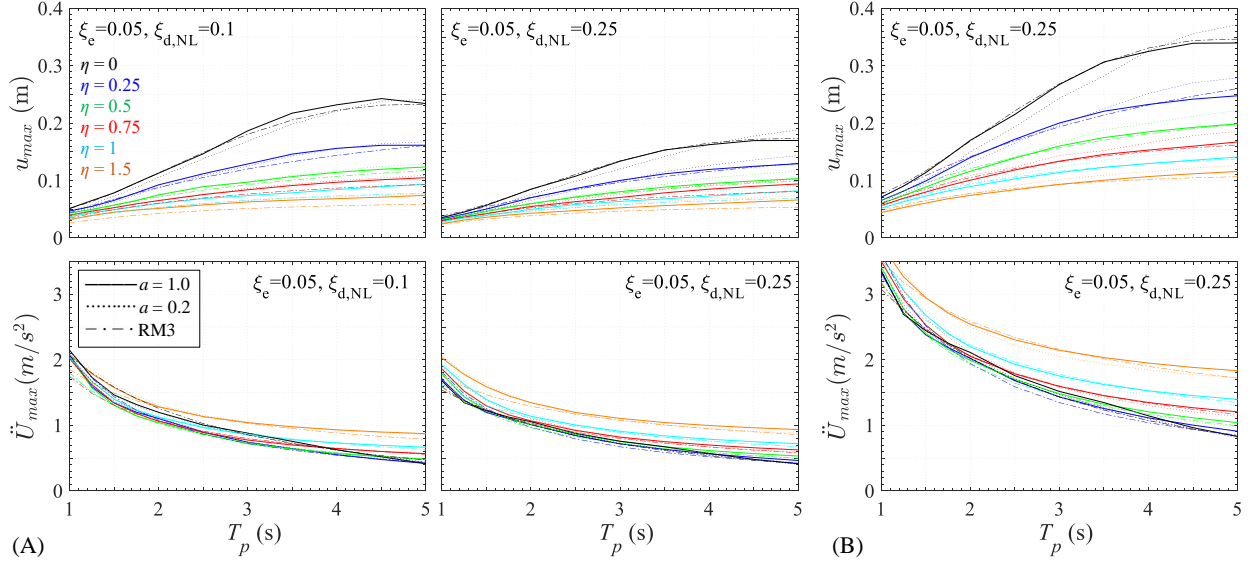

Figure 11 NLRHA response $u_{\max}$ and $\ddot{U}_{\max}$ under Art B considering energy-equivalent dampers of a=1, 0.2, compared to RM3 predicted response for PGA of (A) 0.21g (T_R=475 yrs), and (B) 0.42g ($T_R \approx$2500 yrs) at bedrock, ξ=15, 30%, η=0~1.5

5. ISOLATED 2DOF WITH LINEAR VISCOUS DAMPING

5.1. Dynamic Equation of Motion

The proposed procedure is extended here to investigate the effect of bidirectional excitation on the peak response of isolated 2DOF systems with LVDs. Although 2DOF systems with nonlinear damping are not explicitly checked, the minor effect of nonlinearity of dampers in $u_{\max}$, $\ddot{U}_{\max}$ under unidirectional excitation implies that the relevant equations (and GDEs) presented in the following sections can yield reasonable estimates of peak response in systems involving NLVDs too. In this context, the dynamic equation of motion for the idealised system is re-written considering two dynamic degrees of freedom along two horizontal axes and identical mass (m), stiffness (k_p), isolator strength (V_0) and damping ($c_{e,L}$, $c_{d,L}$) characteristics in both directions. Substituting in each horizontal direction the shear force of the bilinear isolator, the axial force of the LVD, and considering bidirectional interaction between the isolator yield forces with a circular yield surface (i.e. $|z| \leq 1$),[49] result in Equation 16 (symbols in bold represent vectors). Dividing Equation 16 by u_r and substituting $c_{e,L}$, $c_{d,L}$, reduce the equation to the normalised form of Equations 17, 18;

$$\ddot{\boldsymbol{u}}(t) + \left[\frac{\left(c_{e,L} + c_{d,L} \right)}{m} \dot{\boldsymbol{u}}(t) \right] + \left[\bar{v}_0 g \boldsymbol{z}\left(t, k_e, \boldsymbol{u}, \dot{\boldsymbol{u}} \right) + \omega_p^2 \boldsymbol{u}(t) \right] = -\ddot{\boldsymbol{u}}_{\boldsymbol{g}}(t) \tag{16}$$

$$\begin{bmatrix} \ddot{\bar{u}}_x(t) \\ \ddot{\bar{u}}_y(t) \end{bmatrix} + 2\omega_p \left(\xi_{e,L} + \xi_{d,L} \right) \begin{bmatrix} \dot{\bar{u}}_x(t) \\ \dot{\bar{u}}_y(t) \end{bmatrix} + \omega_p^2 \left(\begin{bmatrix} z_x\left(t, k_e, \boldsymbol{u}, \dot{\boldsymbol{u}} \right) \\ z_y\left(t, k_e, \boldsymbol{u}, \dot{\boldsymbol{u}} \right) \end{bmatrix} + \begin{bmatrix} \bar{u}_x(t) \\ \bar{u}_y(t) \end{bmatrix} \right) = -\left(\omega_p^2 / \eta \omega_D \right) \begin{bmatrix} \ddot{\bar{u}}_{gx}(t) \\ \ddot{\bar{u}}_{gy}(t) \end{bmatrix} \tag{17}$$

$$\ddot{\bar{\boldsymbol{u}}}(t) = \ddot{\boldsymbol{u}}(t)/u_r , \ \dot{\bar{\boldsymbol{u}}}(t) = \dot{\boldsymbol{u}}(t)/u_r , \ \bar{\boldsymbol{u}}(t) = \boldsymbol{u}(t)/u_r , \ \ddot{\bar{\boldsymbol{u}}}_{\boldsymbol{g}}(t) = \ddot{\boldsymbol{u}}_{\boldsymbol{g}}(t)/\dot{u}_{g,\max,2D} \tag{18}$$

The normalised strength η is defined according to Equation 9, where $\dot{u}_{g,\max}$ is substituted with $\dot{u}_{g,\max,2D}$. The latter quantity, characterising the seismic intensity of a pair of horizontal components, is defined as the PGV of the SRSS spectrum (of the pair of records) scaled to the 1D target spectrum (Figure 2B). $\dot{u}_{g,\max,2D}$ is estimated from Equation 19; this definition is preferred over '*the PGV of the stronger component of ground motion*'[5,6] for reasons of compatibility with the target spectra and the scaling approach adopted in Section 2, hence, with relevant code-based requirements.[8] Specifically, Equation 19 enables direct comparisons of response quantities derived from analysis under unidirectional and bidirectional excitation, since in both cases a specific η value will correspond to (nearly) the same isolation system strength $\bar{v}_0$.

$$\dot{u}_{g,\max,2D} = \sqrt{\dot{u}_{g,\max,x}^{~~2} + \dot{u}_{g,\max,y}^{~~2}} \Big/ \sqrt{2} \tag{19}$$

The peak inelastic normalised and non-normalised response under bidirectional excitation is defined according to Equation 20 (using non-normalised quantities in the second case) as the peak values of the response histories derived by adding at each time-step the relevant response vectors along the x and y axes. The angles at which the relevant peak response quantities are developed are identical in the cases of non-normalised and normalised response (i.e. independent of the normalisation procedure) and are calculated from Equation 21 with respect to the x axis, where t_i, t_j represent the time instances at which $\bar{u}_{\max,2D}$ and $\ddot{\bar{U}}_{\max,2D}$ are recorded;

$$\bar{u}_{\max,2D} = \max_t \sqrt{\bar{u}_x(t)^2 + \bar{u}_y(t)^2}, \quad \ddot{\bar{U}}_{\max,2D} = \max_t \sqrt{\ddot{\bar{U}}_x(t)^2 + \ddot{\bar{U}}_y(t)^2} \tag{20}$$

$$\theta_{\bar{u}_{\max}} = \tan^{-1}\left(\left|\frac{\bar{u}_y(t_i)}{\bar{u}_x(t_i)}\right|\right) = \theta_{u_{\max}}, \quad \theta_{\ddot{\bar{U}}_{\max}} = \tan^{-1}\left(\left|\frac{\ddot{\bar{U}}_y(t_j)}{\ddot{\bar{U}}_x(t_j)}\right|\right) = \theta_{\ddot{U}_{\max}} \quad \left(0 \le \theta \le 90^o\right) \tag{21}$$

The following numerical study investigates the efficiency of the normalisation procedure in uncoupling $\bar{\boldsymbol{u}}$, $\ddot{\bar{\boldsymbol{U}}}$ from the ground motion amplitude, and presents some useful comparisons of peak response under unidirectional and bidirectional excitation.

5.2. Parametric Analysis of 2DOF System

The numerical study of Section 3.2 is repeated here for the Art D, and Nat(SRSS) ($\gamma_{EC8} = 1$) suites. Upper values of *SEGM* in the case of Art D were found lower than 15% with a 90% *CL* in the case of $\bar{u}_{\max}$ and lower than 10% in the case of $\ddot{\bar{U}}_{\max}$ similarly to unidirectional excitation, apart from $\eta = 1.50$ that exhibits peak values of *SEGM* for $\bar{u}_{\max}$ around 20% ($\delta \approx 0.3$). This is an indication that an increase in the number of artificial records may be required to attain the same degree of reliability with unidirectional excitation for increased η values. The amplitude of ground motion had once again a negligible effect on the normalised peak response resulting in $\bar{u}_{\max}$, $\ddot{\bar{U}}_{\max}$ curves[30] similar to those in Figure 6 (but of higher magnitude), indicating the effectiveness of the normalisation procedure. Relevant implications emerging from the use of natural records apply also in the case of bidirectional excitation. Increased computational effort involving a larger number of records and analyses will be required to attain the same degree of reliability with the case of artificial records, and effectively control the shape and the PGV of the mean spectrum of the selected records to match the target spectra and design PGV. Figure 12 reveals that adopting the Nat(SRSS) suite underestimates $u_{\max}$ and $\ddot{U}_{\max}$, similarly to Figure 7, due to the adoption of a design PGV that is smaller than the *GM* of record *PGV*s (i.e. 0.353m/s for $T_R = 475$ yrs, derived from Equation 19).

Figure 13A presents a comparative evaluation of $u_{\max}$ and $\ddot{U}_{\max}$ resulting from NLRHA under unidirectional and bidirectional excitation associated with $T_R \approx 2500$ yrs. A significant increase in peak response estimates is observed in the case of bidirectional excitation wherein $u_{\max}$ and $\ddot{U}_{\max}$ incorporate the effect of the transverse component of seismic action according to Equation 20. More importantly, Figure 13A displays the expected increase in $u_{\max}$ and $\ddot{U}_{\max}$ when the 2D target spectrum is defined according to EN1998–2.[8] It should be noted that the adopted intensity ratio of the horizontal component spectra (i.e. $\gamma_{H2} / \gamma_{H1} = 0.75$) was found to have a rather insignificant effect on the peak resultant response derived from Equations 20 (e.g. compared to the case of $\gamma_{H2} / \gamma_{H1} = 1.0$). In fact, the ratio of 0.75 was selected to evaluate in a more realistic context[32] the angle of peak response quantities. Furthermore, design codes (e.g. [8,9])

usually constraint response spectrum and nonlinear dynamic analysis results by relevant response quantities calculated from the *fundamental mode method*,[8] without providing specific guidelines on the proper consideration of the transverse component in the latter method. Hence, the expected increase in u_{max} and $\ddot{U}_{max}$ can serve as a means to evaluate the consistency of results among different analysis types by appropriately scaling the response calculated from the *fundamental mode method*; in this context, it is quantified with the aid of regression analysis in Section 5.3.
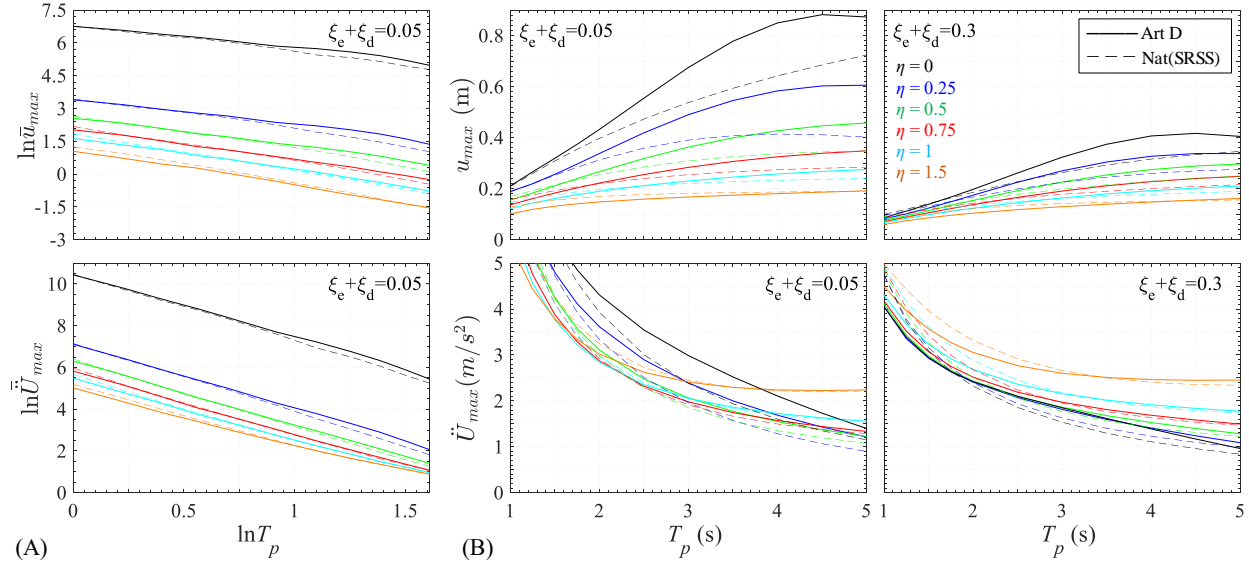

Figure 12 NLRHA results under Art D, Nat(SRSS) (γ_{EC8}=1) suites: *GM* of (A) $\ln\bar{u}_{max}$, $\ln\ddot{\bar{U}}_{max}$, and (B) u_{max}, $\ddot{U}_{max}$, for *PGA*=0.42g (T_R≈2500 yrs, γ_{EQ}=2) at bedrock, ξ=5, 30%, and η=0~1.5
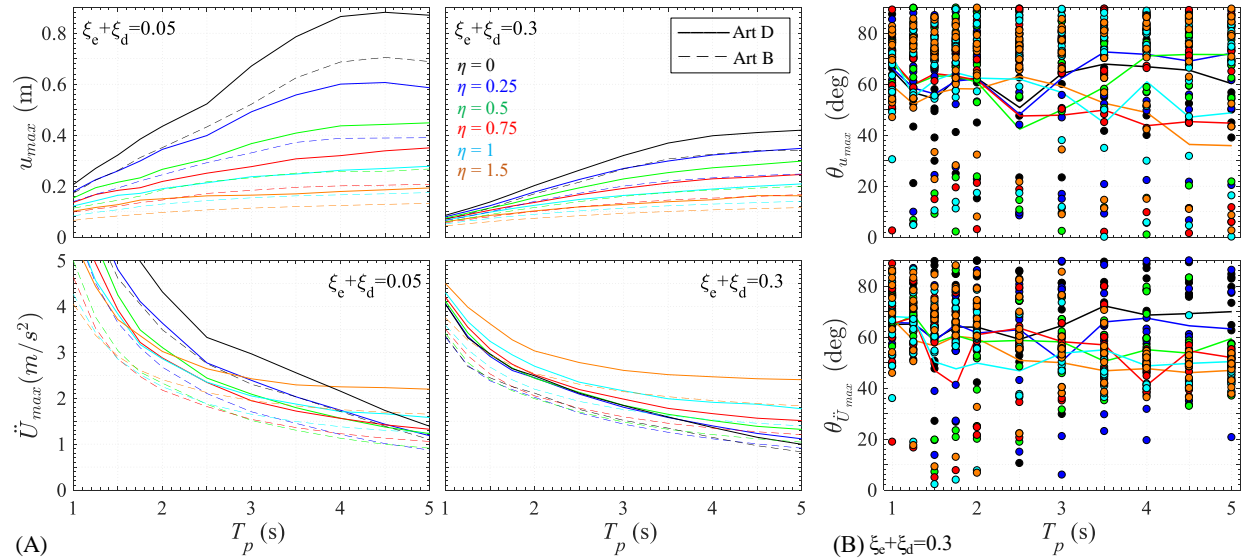

Figure 13 NLRHA results under Art B, Art D (H1 assigned to *y* axis): (A) *GM* of u_{max}, $\ddot{U}_{max}$; (B) angles θ with respect to *x* axis (discrete dots) and *GM* of θ per η for u_{max}, $\ddot{U}_{max}$, *PGA*=0.42g (T_R≈2500 yrs) at bedrock, ξ=5, 30% and η=0~1.5

Returning to the issue of the angle of peak response, Figure 13B reports $\theta_{u_{max}}$, $\theta_{\ddot{U}_{max}}$ values derived from parametric analysis using Art D and Equation 21; solid lines represent *GM* of observed values from analyses under the 10 pairs of records, and solid dots recorded values per individual analysis. Interestingly, mean angles are stabilised close to the value associated with the intensity ratio of horizontal components adopted in analysis (i.e. tan^{-1}(1 / 0.75) = 53°) representing approximately the incidence angle of the resultant of components. However, the reliability of the mean

values is significantly low with peak *SEGM* in u_{max}, $\ddot{U}_{max}$ values exceeding 100% due to the increased scattering of observations. Clear response patters cannot be identified and $\theta_{u_{max}}$, $\theta_{\ddot{U}_{max}}$ may take any value within 0–90°; this justifies and encourages the common practice of designing isolators to sustain the peak relative displacement in any random direction (which unfortunately is not always required by codes, e.g. [8]). It further indicates the need for applying the selected records at different angles of incidence when designing the substructure of isolated bridges, unless a more conservative approach is adopted. Results from analysis using the suite of natural records support the previous statements.

5.3. Derivation of Generalised Design Equations

Regression models and associated GDEs for the case of bidirectional excitation were first developed, and subsequently assessed in terms of accuracy in peak response prediction and effectiveness in 'near-optimal' system identification for practical applications.[30] The efficiency of the adopted model (i.e. RM3) in predicting the peak inelastic response is demonstrated in Figure 14. GDEs in this case (RM3, elastomer-based isolators and a target spectrum with site conditions 'C'[25]), take the general form of Equations 11, 12 simplified as shown in Table 2. The ground motion intensity is expressed in terms of PGA at bedrock (m/s²) of the target spectrum under unidirectional excitation (Equation 19).
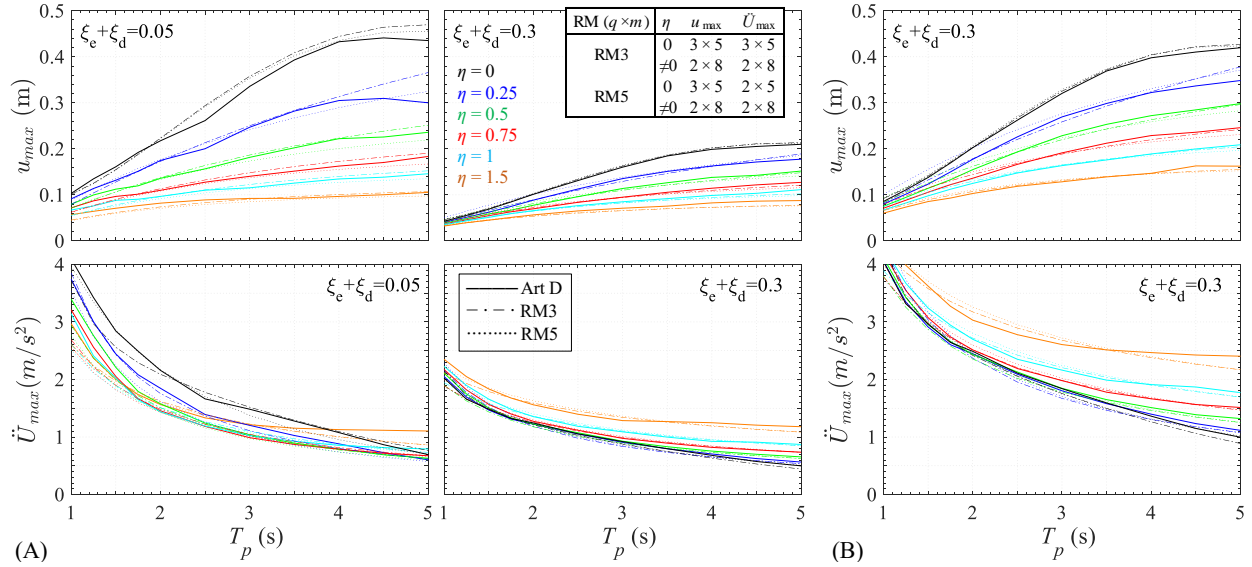

Figure 14 NLRHA response u_{max} and $\ddot{U}_{max}$ under Art D compared to response predicted from RM3 and RM5 for (A) PGA of 0.21g (T_R=475 yrs), (B) PGA of 0.42g ($T_R \approx$2500 yrs) at bedrock, ξ=5, 30%, and η=0~1.5

Table 2 RM3 regression coefficients: EN1998–1, site conditions 'C'[25], 2D excitation.

Case	y	Int	β	γ	δ	ε	ζ	κ	λ	μ	ν
η=0	u_{max}	5.418	-0.440	-	-	-	-	-	-1.206	0.803	-0.438
	$\ddot{U}_{max}$	9.425	-0.305	-	-	-	-	-	-3.165	0.756	-0.399
η=0.25-1.5	u_{max}	0.865	-0.222	0.106	-	-1.126	-0.131	-0.230	-1.074	-0.185	-
	$\ddot{U}_{max}$	4.890	-0.163	0.116	0.152	-0.715	0.157	0.249	-2.335	-	-

Table 3 RM5 regression coefficients: EN1998–1, site conditions 'C'[25], 2D excitation.

Case	y	Int	$\beta, \gamma, \delta, \varepsilon, \zeta, \kappa, \lambda, \mu, \nu$	$u_{max,2D} / u_{max,1D}$ or $\ddot{U}_{max,2D} / \ddot{U}_{max,1D} = e^{Int,2D} / e^{Int,1D}$
$\eta = 0$	u_{max}	5.445		1.22
	$\ddot{U}_{max}$	9.148	Table 1	1.22
$\eta = 0.25\text{-}1.5$	u_{max}	0.978		1.43
	$\ddot{U}_{max}$	5.001		1.26

Representing an alternative to RM3, RM5 model (Table 3, Figure 14) was developed by constraining the regression coefficients (except for the Intercept Int term) to the values obtained from RM3 under unidirectional excitation, as the relevant coefficients were found to be reasonably similar (i.e. Table 2 vs. 1). This approach allows further simplification of the adopted models since the peak response under bidirectional excitation can be calculated from GDEs of unidirectional excitation by scaling relevant response quantities according to the data in Table 3. The provided ratios of peak inelastic response reflect in addition the 'mean increase' in u_{max}, $\ddot{U}_{max}$ due to the introduction of the transverse component of seismic action when target spectra are defined according to EN1998–2,[8] thus, offering an effective means to evaluate results deriving from different types of analysis according to Section 5.2.

6. CONCLUSIONS

A methodology for the direct estimation of peak inelastic response in bilinear isolation systems was extended here with a view to properly capturing the effect of linear/nonlinear viscous damping, and hence addressing a wide range of isolation and energy dissipation configurations. The suggested approach consists of a normalisation procedure aiming at the development of generalised design equations (GDEs) capable of providing reliable estimates of peak inelastic response under different performance levels associated with code-based target spectra of common frequency content but different amplitude. Three different cases were explicitly considered, namely, (*i*) isolated SDOF systems with linear and (*ii*) nonlinear viscous damping, and (*iii*) isolated 2DOFs with linear viscous damping, representing idealised isolated bridge decks under unidirectional and bidirectional excitation. The following conclusions, regarding the development of the methodology and its usefulness in practical applications, were drawn from extensive parametric nonlinear dynamic analyses:

- The dynamic equation of motion was normalised, aiming at uncoupling the normalised response from the amplitude of ground motion and limiting the dispersion in peak normalised relative displacements $\bar{u}_{max}$ and total accelerations $\ddot{\bar{U}}_{max}$. Two conditions were introduced in this respect. The first condition involved the characterisation of the isolation system strength by η (i.e. strength at zero displacement V_0 normalised to the ground motion intensity as expressed by PGV). The second was associated with the characterisation of nonlinear viscous dampers by the 'energy-equivalence' approach (i.e. dampers of the same damping ratio ξ but different velocity exponent a). The above conditions along with the assumption of a constant value for the yield displacement reduce the governing parameters that significantly affect the response, to the isolation period T_p, η, and ξ. Further, they allow the development of GDEs (with the aid of regression analysis) for the direct estimation of non-normalised relative displacements u_{max} and total accelerations $\ddot{U}_{max}$, since the maximum force of the isolation and energy dissipation system cannot be directly associated with u_{max}. The developed regression models were assessed both in terms of accuracy in peak response prediction and effectiveness in 'near-optimal' system identification, while the procedure was fully automated within a developed *MATLAB* code to facilitate the development of GDEs in cases different from those considered herein.

- Tailoring to the needs of practical design by means of using code-type target spectra and scaling procedures, entails the selection and/or generation of records with mean characteristics (i.e. mean spectrum, mean PGV) that closely match the target properties (i.e. shape of target spectrum, design PGV). The above requirements are associated with increased computational effort when natural records are used. On the other hand, artificial accelerograms (notwithstanding their known pitfalls)[50] may easily satisfy the above requirements and provide robust estimates of mean response when member strength degradation is not considered. Alternative 'spectrum-matching' approaches (e.g. [51]) will be explored in future studies.

- In the case of bidirectional excitation, the large dispersion in the angles at which peak response occurs, justifies and encourages the common practice of designing isolators to sustain u_{max} in any random direction; it also points

to the need for applying the selected records at different angles of incidence when designing the substructure. Development of regression models by constraining the regression coefficients of relevant models under unidirectional excitation, provided magnification factors that offer an effective means to evaluate results derived from different types of analysis according to code requirements.

Considering that GDEs can be extracted for prescribed target spectra and provided as ready-to-use design tools, the suggested procedure represents an alternative to equivalent linearisation approaches commonly adopted by codes. As such, it can be implemented either as a 'stand-alone' tool in bridges with stiff substructure and insignificant torsional effects, or for preliminary design purposes in more complex systems. In this context, a key aim for developing the proposed procedure is to incorporate it in the *Deformation-Based Design* method for seismically isolated bridges (under uni/bidirectional excitation), as it will be presented in a forthcoming paper.

ACKNOWLEDGMENT

REFERENCES

1. Housner GW, Bergman LA, Caughey TK, et al. Structural control: Past, present, and future. *J Eng Mech*. 1997;123(9):897–971.

2. Priestley MJN, Calvi GM, Kowalsky MJ. *Displacement-Based Seismic Design of Structures*. IT: IUSS Press; 2007.

3. Cardone D, Dolce M, Palermo G. Direct displacement-based design of seismically isolated bridges. *Bull Earthq Eng*. 2009;7(2):391–410.

4. Landi L, Fabbri O, Diotallevi PP. A two-step direct method for estimating the seismic response of nonlinear structures equipped with nonlinear viscous dampers. *Earthq Eng Struct Dyn*. 2014;43(11):1641–1659.

5. Ryan KL, Chopra AK. Estimation of seismic demands on isolators based on nonlinear analysis. *J Struct Eng*. 2004;130(3):392–402.

6. Ryan KL, Chopra AK. Estimating the seismic displacement of friction pendulum isolators based on non-linear response history analysis. *Earthq Eng Struct Dyn*. 2004;33(3):359–373.

7. Guo JWW, Christopoulos C. Performance spectra based method for the seismic design of structures equipped with passive supplemental damping systems. *Earthq Eng Struct Dyn*. 2013;42(6):935–952.

8. Comité Européen de Normalisation (CEN). *Eurocode 8: Design of Structures for Earthquake Resistance - Part 2: Bridges (EN1998–2)*. Brussels, BE: CEN; 2005.

9. American Association of State Highway and Transportation Officials (AASHTO). *Guide Specifications for Seismic Isolation Design*. Washington, DC: AASHTO; 2010.

10. American Society of Civil Engineers (ASCE), Structural Engineering Institute (SEI). *Minimum Design Loads and Associated Criteria for Buildings and Other Structures (ASCE/SEI 7–16)*. Reston, VA: ASCE; 2016.

11. Hwang JS, Sheng LH. Equivalent elastic seismic analysis of base-isolated bridges with lead-rubber bearings. *Eng Struct*. 1994;16(3):201–209.

12. Hwang JS, Chiou JM. An equivalent linear model of lead-rubber seismic isolation bearings. *Eng Struct*. 1996;18(7):528–536.

13. Makris N, Kampas G. The engineering merit of the "effective period" of bilinear isolation systems. *Earthq Struct*. 2013;4(4):397–428.

14. Dicleli M, Buddaram S. Equivalent linear analysis of seismic-isolated bridges subjected to near-fault ground motions with forward rupture directivity effect. *Eng Struct*. 2007;29(1):21–32.

15. Dicleli M, Buddaram S. Comprehensive evaluation of equivalent linear analysis method for seismic-isolated structures represented by sdof systems. *Eng Struct*. 2007;29(8):2653–1663.

16. Jara M, Jara J, Olmos B, Casas J. Improved procedure for equivalent linearization of bridges supported on hysteretic isolators. *Eng Struct*. 2012;35:99–106.

17. Ramirez OM, Constantinou MC, Gomez JD, et al. Evaluation of simplified methods of analysis of yielding structures with damping systems. *Earthq Spectra*. 2002;18(3):501–530.

18. Fadi F, Constantinou MC. Evaluation of simplified methods of analysis for structures with triple friction pendulum isolators. *Earthq Eng Struct Dyn*. 2010;39(1):5–22.

19. Warn GP, Whittaker AS. Performance estimates in seismically isolated bridge structures. *Eng Struct*. 2004;26:1261–1278.

20. Ozdemir G, Constantinou MC. Evaluation of equivalent lateral force procedure in estimating seismic isolator displacements. *Soil Dyn Earthq Eng*. 2010;30:1036–1042.

21. Pant DR, Constantinou MC, Wijeyewickrema AC. Re-evaluation of equivalent lateral force procedure for prediction of displacement demand in seismically isolated structures. *Eng Struct*. 2013;52:455–465.

22. Chopra AK. *Dynamics of Structures: Theory and Applications to Earthquake Engineering*. 4th ed. Upper Saddle River, NJ: Prentice Hall; 2012.

23. Palermo M, Silvestri S, Landi L et al. Peak velocities estimation for a direct five-step design procedure of inter-storey viscous dampers. *Bull Earthq Eng*. 2016;14(2): 599–619.

24. Constantinou MC, Whittaker AS, Fenz DM, Apostolakis G. (2007a) *Seismic Isolation of Bridges*. Buffalo, NY: University at Buffalo; 2007. Project Report 65A0174.

25. CEN. *Eurocode 8: Design of Structures for Earthquake Resistance - Part 1: General Rules, Seismic Actions and Rules for Buildings (EN1998–1)*. Brussels, BE: CEN; 2004.

26. Weatherill G, Crowley H, Danciu L. *Preliminary Reference Euro-Mediterranean Seismic Hazard Zonation*. Zürich, CH: Swiss Seismological Service; 2013. *Seismic Hazard Harmonization in Europe (SHARE)*; Project Deliverable 2.7.

27. Gasparini DA, Vanmarcke EH. *Simulated Earthquake Motions Compatible with Prescribed Response Spectra*. Cambridge, MA: Massachusetts Institute of Tech.; 1976. *Evaluation of Seismic Safety of Buildings*; Report 2.

28. Saragoni GR, Hart GC. Simulation of artificial earthquakes. *Earthq Eng Struct Dyn*. 1973;2(3):249–267.

29. Seismosoft. *SEISMOARTIF: A Computer Program for Generation of Artificial Earthquake Accelerograms*. Pavia, IT: Seismosoft; 2016.

30. Gkatzogias KI. *Performance-Based Seismic Design of Concrete Bridges for Deformation Control through Advanced Analysis Tools and Control Devices*. PhD Dissertation. London, UK: City, University of London; 2017.

31. Penzien J, Watabe M. Characteristics of 3-dimensional earthquake ground motions. *Earthq Eng Struct Dyn*. 1974;3(4):365–373.

32. López OA, Hernández JJ, Bonilla R, Fernández A. Response spectra for multicomponent structural analysis. *Earthq Spectra*. 2006;22(1):85–113.

33. Katsanos EI, Sextos AG. ISSARS: An integrated software environment for structure-specific earthquake ground motion selection. *Adv Eng Softw*. 2013;58:70–85.

34. Ancheta DT, Darragh RB, Stewart JP, et al. *PEER NGA-West 2 Database*. Berkeley, CA: Pacific Earthquake Engineering Research Center (PEER); 2013. Report 2013/03.

35. PEER. *Technical Report for the PEER Ground Motion Database Web Application*. Berkeley, CA: PEER; 2011.

36. Rezaeian S, Der Kiureghian A. Simulation of orthogonal horizontal ground motion components for specified earthquake and site characteristics. *Earthq Eng Struct Dyn*. 2012;41(2):335–353.

37. Carr AJ. *RUAUMOKO 3D: Inelastic Dynamic Analysis Program*. Christchurch, NZ: University of Canterbury; 2004.

38. Mathworks. *MATLAB and Statistics Toolbox*. Release 2016b. Natick, MA: The MathWorks, Inc.; 2016.

39. Carr AJ. *RUAUMOKO DYNAPLOT: Dynamic Analysis Results Post-Processor*. Christchurch, NZ: University of Canterbury; 2004.

40. Wen YK. Approximate method for nonlinear random vibration. *J Eng Mech Div*. 1975;101(4):389–401.

41. Wen YK. Method for random vibration of hysteretic systems. *J Eng Mech Div*. 1976;102(2):249–263.

42. Makris N, Chang SP. Effect of viscous, viscoplastic, and friction damping on the response of seismic isolated structures. *Earthq Eng Struct Dyn*. 2000;29(1):85–107.

43. Makris N, Vassiliou MF. The existence of 'complete similarities' in the response of seismic isolated structures subjected to pulse-like ground motions and their implications in analysis. *Earthq Eng Struct Dyn*. 2011;40(10):1103–1121.

44. Symans MD, Constantinou MC. Passive fluid viscous damping systems for seismic energy dissipation. *ISET J Earthq Tech*. 1998;35(4):185–206.

45. Lin WH, Chopra AK. Earthquake response of elastic SDF systems with non-linear fluid viscous dampers. *Earthq Eng Struct Dyn*. 2002;31(9):1623–1642.

46. Hancock J, Bommer JJ, Stafford PJ. Numbers of scaled and matched accelerograms required for inelastic dynamic analyses. *Earthq Eng Struct Dyn*. 2008;37(14):1585–1607.

47. Ray T, Reinhorn AM, Nagarajaiah S. Nonlinear elastic and inelastic spectra with inherent and supplemental damping. *Earthq Eng Struct Dyn*. 2013;42(14):2151–2165.

48. Inaudi JA, Kelly JM. Optimum damping in linear isolation systems. *Earthq Eng Struct Dyn*. 1993;22(7):583–598.

49. Huang WH. *Bi-directional Testing, Modeling, and System Response of Seismically Isolated Bridges*. PhD Dissertation. Berkeley, CA: University of California, Berkeley; 2002.

50. Naeim F, Lew M. On the use of design spectrum compatible time-histories. *Earthq Spectra*. 1995;11(1):111–127.

51. Hancock J, Watson-Lamprey J, Abrahamson NA et al. An improved method of matching response spectra of recorded earthquake ground motion using wavelets. *J Earthq Eng*. 10(S1):67–89.